Published for SISSA by Springer

Received: January 14, 2022
Revised: March 10, 2022
Accepted: March 14, 2022
Published: March 28, 2022

Neutrino masses and magnetic moments of electron and muon in the Zee Model

Rahool Kumar Barman,[a] **Ritu Dcruz**[a] **and Anil Thapa**[b]

[a] *Department of Physics, Oklahoma State University, Stillwater, OK 74078, U.S.A.*
[b] *Department of Physics, University of Virginia, Charlottesville, Virginia 22904-4714, U.S.A.*

E-mail: rahool.barman@okstate.edu, rdcruz@okstate.edu, wtd8kz@virginia.edu

Abstract: We explore parameter space in the Zee Model to resolve the long-standing tension of the electron and muon anomalous magnetic moment (AMM). The model comprises a second Higgs doublet and a charged singlet at electroweak scale and generates Majorana neutrino masses at one-loop level; the neutral partner of the $SU(2)_L$ doublet contributes to the AMM of electron and muon via one loop and two-loop corrections. We propose two minimal flavor structures that can explain these anomalies while fitting the neutrino oscillation data. We find that the neutral Higgs resides in the mass range of roughly 10–300 GeV or 1–30 GeV, depending on the flavor structures. The model is consistent with constraints from colliders, electroweak precision data, and lepton flavor violation. To be comprehensive, we examine the constraints from the electric dipole moment (EDM) and find a region of parameter space that gives a sizable contribution to muon EDM while simultaneously giving corrections to muon AMM. In addition to the light scalar, the two charged scalars with masses as low as 100 GeV can induce nonstandard neutrino interactions ε_{ee} as large as 8%, potentially hinting at new physics. We also investigate the projected capability of future lepton colliders to probe the currently allowed parameter space consistent with both electron and muon AMMs via direct searches in the $\ell^+\ell^- \to \ell^+\ell^-(H \to \ell^+\ell^-)$ channel.

Keywords: Baryon/Lepton Number Violation, Multi-Higgs Models, Other Weak Scale BSM Models, Specific BSM Phenomenology

ArXiv ePrint: 2112.04523

https://doi.org/10.1007/JHEP03(2022)183

JHEP03(2022)183

Contents

JHEP03(2022)183

1 Introduction

Understanding the origin of neutrino masses to explain the firmly established observed neutrino oscillation data [1] stands out among the many reasons to consider Physics beyond the Standard Model (BSM). The tiny neutrino mass can be realized by the dimension-five Weinberg operator [2] that the breaks lepton number by two units and gives Majorana masses to neutrinos after electroweak symmetry breaking. This operator can be realized at tree level by adding SM-singlet fermions via a type-I seesaw mechanism [3–7], adding

an $SU(2)_L$-triplet scalar [8–11] via type-II, or $SU(2)_L$ triplet fermion [12] via type-III. An alternative and interesting scenario where small neutrino masses arise naturally are through quantum corrections [9, 13–15] (For a review, see refs. [16, 17]). The new degrees of freedom that generate neutrino mass in these radiative models cannot be too heavy, and therefore, they can be accessible for the experimental test at colliders. Moreover, these new particles typically give rise to enhanced lepton flavor violating (LFV) signals such as $\mu \to e\gamma$ and $\tau \to 3\mu$. Here we revisit the Zee Model [13], the simplest extension of SM that contains an extra doublet scalar and a singly-charged scalar that can generate Majorana neutrino mass at a one-loop level. The new Higgs doublet present in the model can also play an important role in explaining persistent experimental anomalies, viz., the anomalous magnetic moment (AMM) of muon (Δa_μ) and electron (Δa_e).

The long-standing discrepancy between the experiment and theory in the anomalous magnetic moment of lepton a_ℓ hints at physics beyond the SM, where $a_\ell = (g_\ell - 2)/2$ in SM is calculated from perturbative expansion in the fine-structure constant α_{em}. For instance, the one-loop QED effect [18, 19] gives a deviation of 0.1% from the Dirac prediction in the Landé g-factor at tree level $g = 2$. The contribution to a_ℓ^{SM} arises from loops containing Quantum Electrodynamics (QED) corrections, hadronic (QCD) processes, and electroweak (EW) pieces. The QED calculations [20–37] have been carried out up to and including $\mathcal{O}(\alpha_{em}^5)$ while electroweak corrections [38–44] have been evaluated at full two-loop order with negligible uncertainty, arising mainly from nonperturbative effects in two-loop diagrams involving the light quarks. Note that the dominant sources of theoretical uncertainty in AMM arise from the hadronic contributions [45–55], in particular, the $\mathcal{O}(\alpha_{em}^2)$ Hadronic Vacuum Polarization (HVP) term [56–62] and the $\mathcal{O}(\alpha_{em}^3)$ hadronic light-by-light (HLbL) [62–85] term.

The current measurement of AMM of muon a_μ at Fermilab National Accelerator Laboratory (FNAL) reports $a_\mu(\text{FNAL}) = 116592040(54) \times 10^{-11}$ [86], which agrees with the previous Brookhaven National Laboratory (BNL) E821 measurement [87, 88], while theoretical prediction finds it to be $a_\mu^{\text{SM}} = 116591810(43) \times 10^{-11}$ [60, 89–91]. The difference, $\Delta a_\mu = a_\mu(\text{experiment}) - a_\mu(\text{theory}) \simeq (251 \pm 59) \times 10^{-11}$, is a 4.2σ discrepancy. In addition to muon AMM, similar discrepancy of $\sim 2.4\sigma$ between the experimental [92, 93] and theoretical prediction [35, 89, 94–96] of electron AMM has been observed, $\Delta a_e = (-8.8 \pm 3.6) \times 10^{-13}$. These deviations may hint at new physics lying around or below the TeV scale. It is worth mentioning that a more recent measurement of the fine structure constant using Rubidium atoms [97] instead of Cesium atoms has led to a 1.6σ discrepancy of the AMM, but in the opposite direction; $\Delta a_e = (4.8 \pm 3.0) \times 10^{-13}$. This is in complete disagreement with the previous result for unknown reasons. Since there is an ambiguity between the two measurements, we stick with the previous measurement in this work. Although it is not difficult to explain one of the Δa_ℓ in BSM models, it is challenging to explain both simultaneously because of opposite signs of the two AMMs. Various mechanisms have been proposed to explain these deviations; by invoking vector-like fermions [98–106], introducing new scalars [106–120], leptoquarks [121–124], extending the gauge symmetry [125–130], considering non-local QED effects [131] and in the context of supersymmetry [132–138]. Moreover, there are various attempts in the literature that use Higgs doublet models (THDM) to explain both the anomalies [139–142]. We pursue similar in spirit as done in THDM,

JHEP03(2022)183

but unlike THDM, we address these anomalies in the context of radiative neutrino masses in the Zee Model that gives direct connection to the neutrino massses and oscillations.

The flavor-changing nature of the second Higgs doublet that gives rise to large contributions to a_ℓ also plays a crucial role in neutrino masses and oscillations, which reveals insights into the flavor structure within the model. The opposite signs of the anomalies can be explained by either choosing Yukawa couplings with opposite signs or adjusting the mass splitting between the scalars so that Δa_μ is positive from the dominant one-loop diagram. In contrast, the two-loop Barr-Zee diagram provides negative correction to a_e. We propose two minimal Yukawa textures that achieve these while also providing excellent fits to the neutrino oscillation parameters. We find that the simultaneous explanation of the observed disparities in the lepton AMMs requires the scalar mass to be in the range of 10–300 GeV for `TX-I` and 1–30 GeV for `TX-II` while satisfying various LFV measurements such as $\ell_1 \to \ell_2\gamma$, including other relevant constraints from low energy physics, collider searches, and fit to the neutrino oscillation data. It is also worth noting that the Yukawa couplings, if complex, can not only generate a_ℓ but could also have a sizable effect on the electric dipole moment (EDM) d_ℓ. We find that an extremely small complex phase of $\mathcal{O}(10^{-5})$ is required to satisfy the current limits of electron EDM [143] while simultaneously satisfying a_e. However, this is not the case for muon EDM [144], as there exist regions of parameter space that can give a sizable contribution to muon EDM, which can potentially be measured in future experiments [145–147]. The charged scalars in the model can induce nonstandard neutrino interactions (NSI) ε_{ij} [148–150] (for a recent review on NSI in the context of the Zee Model, see ref. [17]), which, if observed, could be direct indicators for new physics. We find that diagonal NSI can be as large as 8% for ε_{ee}.

We have also evaluated constraints on the Yukawa couplings for both the textures from direct searches in the $e^+e^- \to \ell^+\ell^-(H \to \ell^+\ell^-)$ $(\ell = e, \mu)$ channel at LEP. Moreover, we also explore the future sensitivity of the channel, as mentioned earlier, to the Yukawa couplings at the ILC operating at $\sqrt{s} = 1$ TeV with an integrated luminosity $\mathcal{L} = 500$ fb^{-1} [151–155]. We also study the projected sensitivity of the $\mu^+\mu^- \to \mu^+\mu^-$ $(H_2 \to \mu^+\mu^-)$ channel at a muon collider (MuC) with configuration:$\sqrt{s} = 3$ TeV, $\mathcal{L} = 1$ ab^{-1} [156, 157]. These searches could preclude simultaneous explanation of both AMMs in the mass range of roughly 10–300 GeV depending on the Yukawa coupings for a given texture within the model.

The rest of the paper is organized as follows. In section 2 we present the basic description of the Zee Model, including the Yukawa lagrangian and radiative neutrino mass generation. In section 3 we discuss the anomalous magnetic moments and the possible ways of resolving the two anomalies simultaneously in the model. This section also points out the model predictions for muon EDM (cf. section 3.1). Section 4 briefly summarizes the NSI from charged scalars in the model, followed by a detailed study of the various textures of Yukawa coupling matrices which could incorporate both anomalies in section 6. The low energy constraints such as $\ell_i \to \ell_j\gamma$, trilepton decays, T-parameter constraints, muonium oscillations, and direct experimental constraints are discussed in section 5. In section 7 we perform a detailed cut-based collider analysis at the detector level to estimate the projected capability of future lepton colliders to probe the Yukawa structure of the additional scalar Higgs boson considered in this work. The results of our analysis on the

JHEP03(2022)183

anomalous magnetic moment of lepton and neutrino oscillation fit are given in section 8, followed by the conclusion in section 9.

2 Model description

The Zee Model [13, 158], built on the Two Higgs Doublet Model [159, 160], is perhaps the simplest extension of the SM that can generate non-zero radiative neutrino mass at a one-loop level. The model is based on SM gauge symmetry $\mathrm{SU}(3)_C \times \mathrm{SU}(2)_L \times \mathrm{U}(1)_Y$ and consists of a $\mathrm{SU}(2)_L$ doublet scalar H_2 in addition to an SM Higgs doublet H_1 and a charged singlet scalar $\eta^\pm$. In Higgs basis [161], where only the neutral component of H_1 takes a vacuum expectation value (VEV), $\langle H_1^0 \rangle = v \simeq 246\,\mathrm{GeV}$, the doublets can be represented as

$$H_1 = \begin{pmatrix} G^+ \\ \frac{1}{\sqrt{2}}\left(v + H_1^0 + iG^0\right) \end{pmatrix}, \quad H_2 = \begin{pmatrix} H_2^+ \\ \frac{1}{\sqrt{2}}\left(H_2^0 + iA\right) \end{pmatrix}, \tag{2.1}$$

where (G^+, G^0) are the Goldstone modes, (H_1^0, H_2^0) and A are the neutral $\mathcal{CP}$-even and $\mathcal{CP}$-odd scalars, and H_2^+ is a charged scalar field. In the $\mathcal{CP}$ conserving limit, where the quartic couplings are real, the field A decouples from $\{H_1^0, H_2^0\}$. Then one can rotate the $\mathcal{CP}$-even states into a physical basis $\{h, H\}$, where the mixing angle parametrized as

$$\begin{pmatrix} h \\ H \end{pmatrix} = \begin{pmatrix} \cos\widetilde{\alpha} & \sin\widetilde{\alpha} \\ -\sin\widetilde{\alpha} & \cos\widetilde{\alpha} \end{pmatrix} \begin{pmatrix} H_1^0 \\ H_2^0 \end{pmatrix}, \tag{2.2}$$

is given by

$$\sin 2\widetilde{\alpha} = \frac{2\lambda_6 v^2}{m_H^2 - m_h^2}\,. \tag{2.3}$$

Here λ_6 is the quartic coupling of the term $H_1^\dagger H_1 H_1^\dagger H_2$. We base our analysis under the alignment/decoupling limit [162–165], when $\widetilde{\alpha} \to 0$, agreeing with the LHC Higgs data [166, 167], and identify h as the observed 125 GeV SM-like Higgs. Similarly, the charged scalars $\{H_2^+, \eta^+\}$ mix and give rise to the physical charged scalar mass eigenstates $\{h^+, H^+\}$

$$\begin{pmatrix} h^+ \\ H^+ \end{pmatrix} = \begin{pmatrix} \cos\varphi & \sin\varphi \\ -\sin\varphi & \cos\varphi \end{pmatrix} \begin{pmatrix} \eta^+ \\ H_2^+ \end{pmatrix}, \tag{2.4}$$

with the mixing angle φ defined as

$$\sin 2\varphi = \frac{-\sqrt{2}v\mu}{m_{H^+}^2 - m_{h^+}^2}, \tag{2.5}$$

where, μ is the coefficient of the cubic coupling $H_1^\alpha H_2^\beta \epsilon_{\alpha\beta}\eta^-$ in the scalar potential, with $\epsilon_{\alpha\beta}$ being the $\mathrm{SU}(2)_L$ antisymmetric tensor. This cubic term, along with eq. (2.6), would break the lepton number by two units.

The leptonic Yukawa interaction in the Higgs basis can be expressed as

$$-\mathcal{L}_Y \supset f_{ij} L_i^\alpha L_j^\beta \epsilon_{\alpha\beta}\eta^+ + \widetilde{Y}_{ij}\widetilde{H}_1^\alpha L_i^\beta \ell_j^c \epsilon_{\alpha\beta} + Y_{ij}\widetilde{H}_2^\alpha L_i^\beta \ell_j^c \epsilon_{\alpha\beta} + \text{ h.c.} \tag{2.6}$$

JHEP03(2022)183

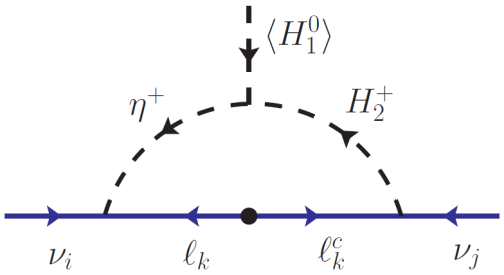

Figure 1. Radiative neutrino mass diagram in the Zee Model. The dot (•) on the SM fermion line represents the mass insertion due to the SM Higgs VEV.

where, $\{i, j\}$ are flavor indices, and $\widetilde{H}_a \equiv i\tau_2 H_a^\star$, τ_2 being the second Pauli matrix. l^c and L represent the left-handed antileptons and lepton doublets. Note, $f_{ij} = -f_{ji}$ is an antisymmetric matrix and can be made real by a phase redefinition $\hat{P}f\hat{P}$, where $\hat{P}$ is a diagonal phase matrix, whereas $\{Y, \widetilde{Y}\}$ are general complex asymmetric matrices. We assume that H_2 is leptophilic to avoid dangerous flavor violating processes in the quark sector, such as $\pi^+ \to e^+\nu$ which would otherwise occur at unacceptably large decay rates for $Y_{ie} \sim \mathcal{O}(1)$. Here, after electroweak symmetry breaking, $M_\ell = \widetilde{Y}\frac{v}{\sqrt{2}}$ is the charged lepton mass matrix, and chosen to be diagonal without loss of generality.

Neutrino masses in this model are zero at the tree level. However, due to explicit lepton number violation, a non-zero Majorana neutrino mass M_ν is induced as quantum corrections at the one-loop level, as shown in figure 1. The dot in the internal fermion line represents the mass insertion due to the SM Higgs VEV. The Yukawa couplings of eq. (2.6), together with the $H_1 H_2 \eta$ trilinear term in the scalar potential, guarantees lepton number violation. These interactions result in an effective ($\Delta L = 2$) $d = 7$ operator $\mathcal{O}_2 = L^i L^j L^k e^c H^l \epsilon_{ij}\epsilon_{kl}$ [17, 168–171]. Note that a companion diagram can be obtained by reversing the arrows of the internal particles. Thus, the neutrino mass matrix is given by

$$M_\nu = \kappa \left(f M_\ell Y + Y^T M_\ell f^T \right), \tag{2.7}$$

where κ is the one-loop factor

$$\kappa = \frac{1}{16\pi^2} \sin 2\varphi \log\left(\frac{m_{h^+}^2}{m_{H^+}^2}\right), \tag{2.8}$$

with φ given in eq. (2.5). It is clear from eq. (2.7) that the product of couplings Y and f is constrained from neutrino oscillation data. For instance, a choice of $Y \sim \mathcal{O}(1)$ compels minuscule Yukawa couplings $f \ll 1$ to generate a tiny neutrino mass of $\mathcal{O}(0.1)$ eV consistent with the current measurements. Thus, such a choice of parameters can correctly reproduce the neutrino oscillation data (see section 8), give the required corrections to the anomalous magnetic moments of electron and muon, and maximize the neutrino NSI in the model.

With the other possibility, namely, $Y \ll 1$, the stringent charge LFV (cLFV) constraints on f Yukawa coupling restrict the maximum NSI to $\leq 10^{-8}$ [172], well below any experimental sensitivity in the foreseeable future. Furthermore, the presence of a singly charged singlet leads to lepton universality violation which, for instance, would alter the decay rate of the

JHEP03(2022)183

muon. The Fermi constant extracted from the modified muon decay would be different from the SM. This new Fermi constant has constraints from the CKM unitarity measurements giving strong limits on the Yukawa couplings, f [16]. The charged current interactions leading to leptonic decays will also be modified so that such interactions are no longer universal, leading to further constraints [173, 174]. Moreover, choosing $Y \ll 1$, one cannot get the required correction to $g-2$ of electron and muon, and η^+ always contributes the wrong sign to the $g-2$ of muon (cf. section 3 for details). The Yukawa couplings f and Y on the mass basis of charged leptons can be written as

$$Y = \begin{pmatrix} Y_{ee} & Y_{e\mu} & Y_{e\tau} \\ Y_{\mu e} & Y_{\mu\mu} & Y_{\mu\tau} \\ Y_{\tau e} & Y_{\tau\mu} & Y_{\tau\tau} \end{pmatrix}, \quad f = \begin{pmatrix} 0 & f_{e\mu} & f_{e\tau} \\ -f_{e\mu} & 0 & f_{\mu\tau} \\ -f_{e\tau} & -f_{\mu\tau} & 0 \end{pmatrix}, \tag{2.9}$$

where Y is multiplied by $(\bar{\nu}_e, \bar{\nu}_\mu, \bar{\nu}_\tau)$ (or (e_L, μ_L, τ_L)) from the left and $(e_R, \mu_R, \tau_R)^T$ from the right in the charged scalar, H^+ (or neutral scalar, $\frac{1}{\sqrt{2}}(H_2^0 + iA)$) interaction. It is worth mentioning that the Yukawa coupling Y cannot be taken diagonal; otherwise, all the diagonal entries of the neutrino mass matrix would vanish, yielding neutrino mixing angles that are not compatible with the neutrino oscillation data [158, 175–177].

3 Anomalous magnetic moments and related process

Virtual corrections due to the new scalar fields present in the model can modify the electromagnetic interactions of the charged leptons. The contribution from $\widetilde{Y}$ of eq. (2.6) is part of the SM contribution, $a_\ell^{\rm SM}$, in the decoupling limit $\tilde{\alpha} = 0$. The contribution from f Yukawa coupling to AMMs is negligible due to the strong limit from cLFV and constrains from tiny neutrino mass, as aforementioned. Thus, the Yukawa Y interactions of leptons with the physical scalars in the alignment limit is given by

$$-\mathcal{L}_Y \supset Y_{ij}\bar{\ell}_{L_i}\ell_{R_j}\phi + Y_{ij}\bar{\nu}_{L_i}\ell_{R_j}H^+ + \text{h.c.}, \tag{3.1}$$

where, $\phi = (H + iA)/\sqrt{2}$. The charged scalar h^+ contribution is ignored by choosing a negligible mixing between charged scalars $\varphi \sim 0$. Neutral scalar contributions to anomalous magnetic moments at one-loop [178] as shown in figure 2(a) is

$$\Delta a_\ell^{(1)}(\phi) = \frac{m_\ell^2}{32\pi^2}\left(\left\{|Y_{\ell i}|^2 + |Y_{i\ell}|^2\right\}F_\phi(x,1) \pm 2\frac{m_i}{m_\ell}\,\mathrm{Re}(Y_{\ell i}Y_{i\ell})F_\phi(x,0)\right), \tag{3.2}$$

where,

$$F_\phi(x,\epsilon) = \int_0^1 \frac{x^2 - \epsilon x^3}{m_\ell^2 x^2 + (m_i^2 - m_\ell^2)x + m_\phi^2(1-x)}\,dx. \tag{3.3}$$

In the above expression, $+$ and $-$ correspond to H and A, respectively, with the second part representing the chiral enhancement. The contribution from charged the Higgs H^+ from figure 2(b) is

$$\Delta a_\ell^{(1)}(H^+) = \frac{m_\ell^2}{16\pi^2}|Y_{i\ell}|^2\int_0^1 \frac{x^3 - x^2}{m_\ell^2 x^2 + (m_{H^+}^2 - m_\ell^2)x}\,dx. \tag{3.4}$$

JHEP03(2022)183

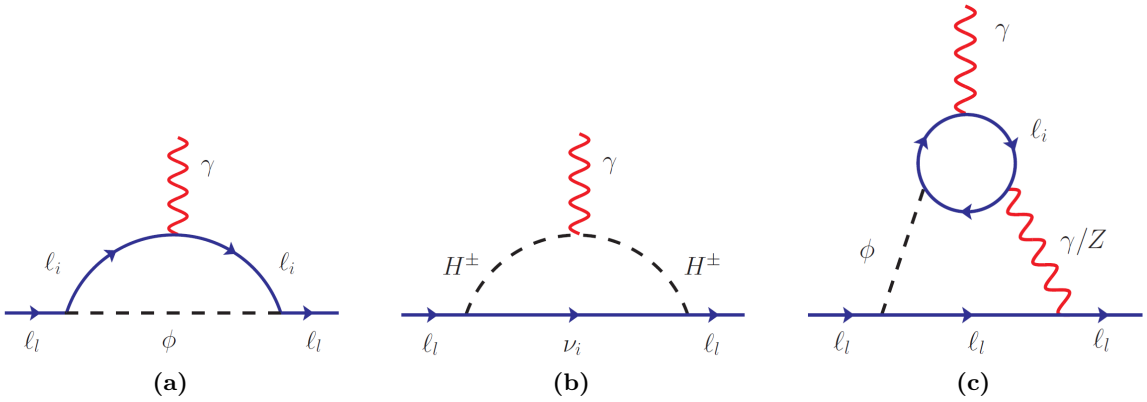

Figure 2. Dominant corrections to a_ℓ in Zee Model. (a) and (b) are one-loop contributions from the scalar sector, and (c) is a typical two-loop Barr-Zee type correction to the AMMs.

The analytical expressions in the limit $m_i \ll m_\phi(m_{H^+})$ for eqs. (3.2) and (3.4) are given in appendix A.1.

There are also two-loop Barr-Zee [179, 180] diagrams arising from the neutral scalars and charged lepton loop [181, 182], as shown in figure 2(c), contributing to the AMM corrections. The two-loop correction is

$$\Delta a_\ell^{(2)} = \frac{\alpha_{em}}{4\pi^3}\frac{m_\ell}{m_i}\frac{z}{2}\Big(- C^\phi_{S_\ell} C^\phi_{S_i} G\,(x,z,1) + C^\phi_{P_\ell} C^\phi_{P_i} G\,(x,z,0)\Big), \tag{3.5}$$

where,

$$G(x,z,\epsilon) = \int_0^1 \frac{1-2\,\epsilon\,x(1-x)}{x(1-x)-z}\log\frac{x(1-x)}{z}\,dx, \tag{3.6}$$

with $z = m_i^2/m_\phi^2$, and the coefficients may be obtained from eq. (3.1) as

$$C^H_{S_i} = C^A_{P_i} = \frac{1}{\sqrt{2}}\mathrm{Re}(Y_{ii}), \quad -C^H_{P_f} = C^A_{S_f} = \frac{i}{\sqrt{2}}\mathrm{Im}(Y_{ii}). \tag{3.7}$$

The analytical expressions for the integrals of eq. (3.6) are given in appendix A.2.

One-loop. First, we investigate the one-loop contribution to $g-2$ of muon and electron from eq. (3.2). As seen from eq. (3.2), for degenerate neutral scalars, i.e., $m_H = m_A$, the chiral enhancement vanishes, making the effective contribution to Δa_l positive. When the couplings are diagonal, a positive contribution to Δa_ℓ can also be achieved by considering $\mathcal{CP}$-odd scalar heavier than $\mathcal{CP}$-even scalar, an ideal scenario to explain Δa_μ. However, such an assumption would contradict with Δa_e, for which an overall negative correction would require a lighter pseudoscalar. It is worth mentioning that the negative contribution from the charged scalar H^+ can partially cancel out the non-chiral part of the neutral scalar corrections. However, the mass of the charged scalar in our choice of the parameter space is always much larger than the mass of the neutral scalar making this effect negligible. Hence, the real Yukawa couplings Y_{ii} $(i = e, \mu)$ cannot explain both the AMMs simultaneously from one-loop corrections. Note that if the lepton mediator is different from the external

JHEP03(2022)183

line $Y_{ij}(i \neq j)$, Yukawa couplings with opposite signs can explain the both the AMMs, subject to constraints from LFV (cf. section 6 and section 5). However, concurrent solutions do exist for $Y_{\mu\mu} \in \mathbb{R} \cap Y_{ee} \in \mathbb{I}$ for $m_A > m_H$ and vice versa for $m_A < m_H$. Note that any nonzero phase in the Yukawa couplings would be constrained by EDMs (cf. section 3.1). The corrections to a_ℓ can appear from one or more of the following Yukawa couplings as shown:

$$\Delta a_\mu \Rightarrow \begin{pmatrix} . & Y_{e\mu} & . \\ Y_{\mu e} & Y_{\mu\mu} & Y_{\mu\tau} \\ . & Y_{\tau\mu} & . \end{pmatrix} + \text{h.c.}, \qquad \Delta a_e \Rightarrow \begin{pmatrix} Y_{ee} & Y_{e\mu} & Y_{e\tau} \\ Y_{\mu e} & . & . \\ Y_{\tau e} & . & . \end{pmatrix} + \text{h.c.}. \tag{3.8}$$

Two-loop. There are several contributions to corrections for AMMs arising at two-loop, which are studied in detail in [181–184]. A typical but most relevant two-loop Barr-Zee diagram is shown in figure 2(c). The contribution from the Z boson line in the figure is typically suppressed by a factor of $\mathcal{O}(10^{-2})$ compared to the photon line. This is partly due to the massive Z boson propagator and the smallness of its leptonic vector coupling, $\frac{g}{\cos\theta_W}(-\frac{1}{4} + \sin^2\theta_W) \sim -0.015$ [185]. Similar diagrams with charged scalars replacing the lepton loop also exist. We suppress, for simplicity, the contribution from this type by considering a small value of quartic coupling λ_7 $(H_2^\dagger H_2 H_1^\dagger H_2)$ in the Higgs potential. Note that this quartic coupling does not contribute to the scalar boson masses. Other diagrams that involve $W^+W^-H_1$ and $H_1H_2H_2$ couplings also vanish in the alignment limit, $\widetilde{\alpha} = 0$ (see figure 3, 5, 6 in ref. [181]). Moreover, there is no $W^+W^-H_2$ and $H_2H_2H_2$ vertex in the Higgs basis where H_2 does not get VEV. The only other non-vanishing diagram, with charged scalars and $W^\pm$ respectively replacing the neutral scalar and photon lines, involves neutrinos. In this case, the loop factor, which is a function of masses of the internal particles, becomes negligible. Interestingly, this diagram becomes considerably dominant if vector-like fermions are involved [182] instead of neutrinos.

Hence, figure 2 (c) is the only two-loop diagram where diagonal Yukawa couplings Y_{ii} are relevant to AMM corrections, as seen from eq. (3.5) and eq. (3.7). Moreover, since there is a chiral enhancement in the lepton loop, $\mathbf{Y}_{\tau\tau}$ contribution becomes relevant. It should be noted that taking $Y_{\tau\tau} \sim 0$, one-loop contribution always dominates two-loop, failing to give concurrent solutions for both AMMs. Here we take $m_H < m_A$ and choose the same sign for Yukawa couplings such that the scalar contribution dominates the pseudoscalar allowing for an overall negative correction to AMMs, thereby providing the right sign to explain Δa_e.

$\Delta a_\mu > 0$ and $\Delta a_e < 0$. The two-loop corrections, even though suppressed by α_{em}/π in comparison to one-loop, have a factor of m_i/m_l from chiral enhancement, as can be seen from eq. (3.5). This plays an important role in providing the right signs to the AMMs. In the case of Δa_e, the factor m_i/m_e enhances the two-loop contribution over the corresponding one-loop correction. Therefore, with a choice of heavier pseudoscalar, the overall correction to Δa_e can be made negative. In doing so, one also gets a negative contribution for Δa_μ enhanced by m_i/m_μ from two-loop, which can become comparable to a one-loop contribution. However, by choosing $Y_{\tau\tau}$ small enough, one can suppress the two-loop contribution and get the correct sign for Δa_μ from one-loop (see section 8.1 for more details).

JHEP03(2022)183

As aforementioned, one-loop by itself can explain both AMMs without the necessity to go to the two-loop level by taking the diagonal couplings $Y_{ii} \sim 0$. In this scenario, one of the Yukawa couplings can be chosen to be negative so that, for a heavier pseudoscalar, the non-chiral part would explain Δa_μ while the chiral part, enhanced by $\log(m_i/m_\phi)$ (cf. (A.1)), explains Δa_e.

3.1 Electric dipole moments

The electric dipole moment of leptons places stringent constraints on the imaginary part of the Yukawa couplings of the scalar field ϕ. We study these constraints by turning on the relevant couplings such that the two-loop contribution becomes subdominant. These constraints are only significant when there is a chirality flip in the fermion line inside the loop, depicted in figure 2(a). In such a scenario lepton EDM is given by [186]

$$d_\ell(\phi) = \frac{\mp q_i m_i}{16\pi^2 m_\phi^2} \frac{\mathrm{Im}(Y_{i\ell}^* Y_{\ell i}^*)}{2} I\left(m_i^2/m_\phi^2, m_\ell^2/m_\phi^2\right), \tag{3.9}$$

with $+(-)$ corresponding to A (H), and

$$I(r,s) = \int_0^1 \frac{x^2}{1 - x + rx - sx(1-x)}\, dx. \tag{3.10}$$

A tiny complex phase of $\mathcal{O}(10^{-5})$ is required to satisfy the current limits on eEDM $|d_e| \leq 1.1 \times 10^{-29}$ e-cm from ACME [143] while also satisfying Δa_e. We can simply avoid the electron EDM limit by taking all the relevant couplings that give rise to Δa_e real. However, for the case of muon EDM, there exist regions of parameter space where the phase of the Yukawa couplings can be significant and provide enough correction to satisfy Δa_μ while also remaining compatible with the current upper limits from eEDM measurements $|d_\mu| \leq 1.9 \times 10^{-19}$ e-cm [144] and can potentially be measurable in future experiments [145–147].

Figure 3 shows the μEDM ranges that can be probed at the near future experiments and satisfy Δa_μ within 1σ for different values of $Y_{\mu\mu} = |Y_{\mu\mu}|e^{i\theta}$. Here we set all the other Yukawa couplings small for simplicity and to satisfy the flavor constraints. Different color bands (red, green, yellow, blue) represent different choices of Yukawa couplings $|Y_{\mu\mu}|$ $(1, 0.1, 0.01, 0.001)$ by allowing the phase to take arbitrary values. The pink and purple shaded regions are excluded from $e^+e^- \to \mu^+\mu^- H$ searches obtained from BABAR [187] and LHC [188], respectively. The bounds were obtained in the $Y_{\mu\mu} - m_H$ plane, which was then projected onto the maximum values of μEDM, obtained at $\theta = \pi/4$. The gray region is excluded from current experiments, and the gray dashed [146] and dotted-dashed lines [145, 147] are the projected sensitivities from various proposed experiments.

It is worth noting that Δa_μ cannot be satisfied for $\theta \in [\frac{\pi}{4}, \frac{3\pi}{4}]$ since the dominant chirally enhanced term in eq. (3.2) is $\propto \cos 2\theta$ which is ≤ 0 for the said region of complex phases regardless of the value of $Y_{\mu\mu}$ and m_H.

JHEP03(2022)183

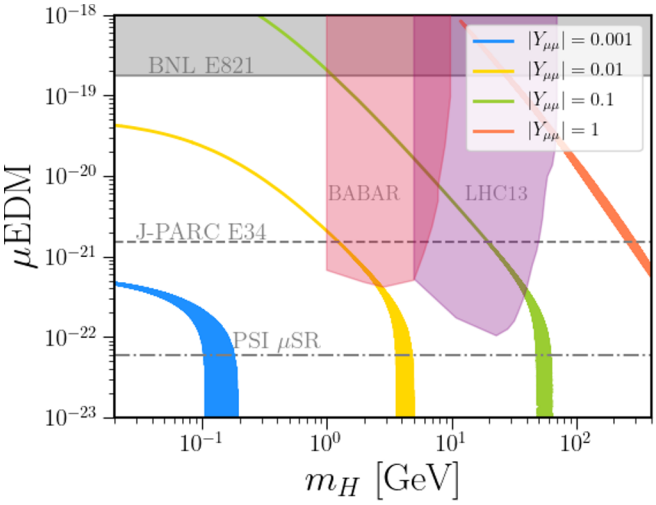

Figure 3. μEDM for different values of Yukawa couplings satisfying Δa_μ at 1σ. The phase of the coupling $Y_{\mu\mu} = |Y_{\mu\mu}|e^{i\theta}$ is taken arbitrarily within $[0, \pi]$. The collider bounds on $Y_{\mu\mu}$ from $e^+e^- \to \mu^+\mu^- H$ searches obtained from BABAR [187](pink) and LHC [188](purple) experiments are projected to the maximum EDM that can be obtained for the coupling. The gray band shows the current experimental bound on μEDM, while the dashed and dotted-dashed gray lines provide the sensitivity reach from future experiments [145–147].

4 Non-standard neutrino interaction

In the Zee Model, the charged scalars η^+ and H_2^+ can induce charged-current NSI at tree level [17]. Since the model can have leptophilic Yukawa couplings Y_{ie} $(i = e, \mu, \tau)$ of order unity, significant NSI can be generated. As mentioned before, $f \ll 1$ due to strong constraints from LFV as well as to correctly reproduce the neutrino oscillation parameters (see section 8). Thus the contributions from f Yukawa couplings are heavily suppressed. Using the dimension-6 operators for NSI [148], the effective NSI parameters in the model can be expressed as

$$\varepsilon_{ij} \equiv \varepsilon_{ij}^{(h^+)} + \varepsilon_{ij}^{(H^+)} = \frac{1}{4\sqrt{2}G_F} Y_{ie} Y_{je}^* \left(\frac{\sin^2\varphi}{m_{h^+}^2} + \frac{\cos^2\varphi}{m_{H^+}^2} \right), \tag{4.1}$$

where h^+ and H^+ are the physical masses of the charged scalars, φ is the mixing angle between the scalars and is define in eq. (2.4) and eq. (2.5). Since we wish to make the neutral scalar light to explain AMM of muon and electron, we take a limit when doublet charged scalar is lighter than singlet charged scalar field. In this limit, the contribution from H^+ dominates, as can be seen, from eq. (4.1). Note that there is a strong constraint from the T-parameter on the choice of neutral and charged scalar masses and mixing among scalars (see section 5.3 for details). Due to the strong constraints from LFV (cf. section 5.1 and section 5.2), one cannot get sizable off-diagonal NSI ε_{ij} $(i \neq j)$ in the model. However, sizable diagonal NSI ε_{ii} can potentially be generated by the matrix elements $(Y_{ee}, Y_{\mu e}, Y_{\tau e})$, contingent on satisfying Δa_ℓ and reproducing neutrino oscillation parameters, which is discussed in the following section.

JHEP03(2022)183

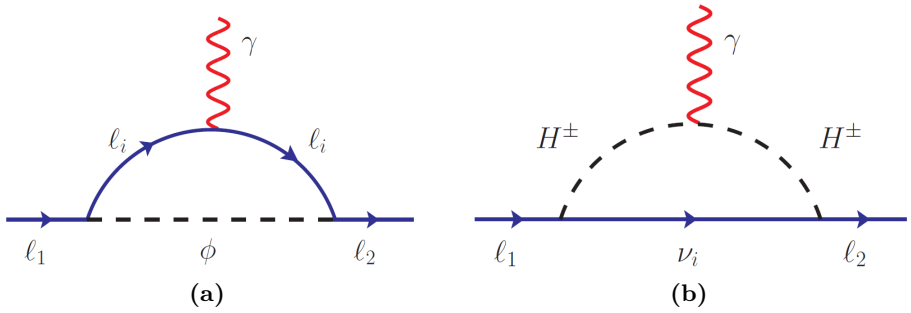

Figure 4. Feynman diagrams inducing radiative decays of charged leptons. ϕ represents both the neutral scalar (H) and pseudoscalar (A).

5 Low-energy constraints

In this section, we summarize various relevant low-energy constraints on the parameter space that can potentially explain the observables being explored here. We can safely ignore charged lepton flavor violation (cLFV) involving the f_{ij} couplings as they are tiny to satisfy the neutrino mass constraint. On the other hand, we require $Y \sim \mathcal{O}(1)$ to explain both AMMs and to induce maximum NSI, which leads to various flavor violating processes that are severely constrained by experimental data.

5.1 $l_1 \to l_2\gamma$

The $l_1 \to l_2\gamma$ decays are induced radiatively at one-loop diagrams as shown in figure 4, and the general expression for such decays involving the neutral scalar field ϕ reads as [189]

$$\Gamma_\phi = \frac{\alpha_{em}}{144\,(16\pi^2)^2}\frac{m_1^5}{16m_\phi^4}\Bigg(\left(\left|Y_{2f}Y_{1f}^*\right|^2 + \left|Y_{f1}Y_{f2}^*\right|^2\right)\mathcal{F}_1^2(t) + \frac{9m_f^2}{m_1^2}\left(\left|Y_{1f}^*Y_{f2}^*\right|^2 + \left|Y_{2f}Y_{f1}\right|^2\right)\mathcal{F}_2^2(t)\Bigg), \tag{5.1}$$

where, for $t = m_f^2/m_\phi^2$,

$$\mathcal{F}_1(t) = \frac{2+3t-6t^2+t^3+6t\log t}{(t-1)^4}, \qquad \mathcal{F}_2(t) = \frac{3-4t+t^2+2\log t}{(t-1)^3}. \tag{5.2}$$

The second term in eq. (5.1) appears from the chirally enhanced radiative diagrams, whereas the first term has no chirality flip in the fermion line inside the loop. The bounds on the Yukawa couplings as a function of the mediator masses are shown in table 1. Table 1 has two rows showing the constraints arising from the chiral enhancement of charged lepton mediator in addition to the diagram without the enhancement. Similarly, the decay rate for $\ell_1 \to \ell_2\gamma$ from charged scalar H^+ in the Zee Model can be expressed as

$$\Gamma_{H^-} = \frac{\alpha_{em}}{144(16\pi^2)^2}\frac{m_1^5}{4m_{H^-}^4}\left|Y_{f1}Y_{f2}^*\right|^2. \tag{5.3}$$

JHEP03(2022)183

Process	Exp. Bound [1]	Constraints
$\mu \to e\gamma$	BR $< 4.2 \times 10^{-13}$ [190]	$\lvert Y_{\mu f} Y_{ef}\rvert^2 + \lvert Y_{f\mu} Y_{fe}\rvert^2 < 1.89 \times 10^{-9} \left(\frac{m_\phi}{100\text{GeV}}\right)^4$
		$(\lvert Y_{ef} Y_{f\mu}\rvert^2 + \lvert Y_{\mu f} Y_{fe}\rvert^2)\ \mathcal{C} < 5.84 \times 10^{-13}\ \left(\frac{m_\phi}{100\ \text{GeV}}\right)^4 \left(\frac{1\ \text{GeV}}{m_f}\right)^2$
$\tau \to e\gamma$	BR $< 3.3 \times 10^{-8}$ [191]	$\lvert Y_{\tau f} Y_{ef}\rvert^2 + \lvert Y_{f\tau} Y_{fe}\rvert^2 < 8.31 \times 10^{-4} \left(\frac{m_\phi}{100\text{GeV}}\right)^4$
		$(\lvert Y_{ef} Y_{f\tau}\rvert^2 + \lvert Y_{\tau f} Y_{fe}\rvert^2)\ \mathcal{C} < 7.29 \times 10^{-5}\ \left(\frac{m_\phi}{100\ \text{GeV}}\right)^4 \left(\frac{1\ \text{GeV}}{m_f}\right)^2$
$\tau \to \mu\gamma$	BR $< 4.4 \times 10^{-8}$ [191]	$\lvert Y_{\tau f} Y_{\mu f}\rvert^2 + \lvert Y_{f\tau} Y_{f\mu}\rvert^2 < 1.11 \times 10^{-3} \left(\frac{m_\phi}{100\text{GeV}}\right)^4$
		$(\lvert Y_{\mu f} Y_{f\tau}\rvert^2 + \lvert Y_{\tau f} Y_{f\mu}\rvert^2)\ \mathcal{C} < 9.72 \times 10^{-5}\ \left(\frac{m_\phi}{100\ \text{GeV}}\right)^4 \left(\frac{1\ \text{GeV}}{m_f}\right)^2$

Table 1. Constraints on Yukawa couplings from radiative decay of charged leptons mediated by neutral scalars, ϕ. Here, $\mathcal{C} = \left(\frac{3}{2} + \log\frac{m_f^2}{m_\phi^2}\right)^2$. For each process, there are diagrams with and without chiral enhancement from different charged lepton mediators, f. The first row in the "Constraints" column shows the bound on the diagram with no chiral enhancement, whereas the second row gives the bound on the chirally enhanced diagram contributed by the charged lepton mediator.

Process	Exp. Bound [1]	Constraints
$\mu \to e\gamma$	BR $< 4.2 \times 10^{-13}$ [190]	$\lvert Y_{f\mu} Y_{fe}\rvert^2 < 1.89 \times 10^{-9} \left(\frac{m_{H^-}}{100\text{GeV}}\right)^4$
$\tau \to e\gamma$	BR $< 3.3 \times 10^{-8}$ [191]	$\lvert Y_{f\tau} Y_{fe}\rvert^2 < 8.31 \times 10^{-4} \left(\frac{m_{H^-}}{100\text{GeV}}\right)^4$
$\tau \to \mu\gamma$	BR $< 4.4 \times 10^{-8}$ [191]	$\lvert Y_{f\tau} Y_{f\mu}\rvert^2 < 1.11 \times 10^{-3} \left(\frac{m_{H^-}}{100\text{GeV}}\right)^4$

Table 2. Constraints on Yukawa couplings from radiative decay of charged leptons mediated by charged scalar, H^-. The constraints here are similar to that of the neutral scalars with no chiral enhancement, given in table 1.

Note that there are no chirally enhanced contributions in these decays. The bounds on the Y Yukawa couplings as a function of the mediator masses are shown in table 2.

5.2 Trilepton decays

The flavor-changing nature of the new scalar bosons allows for the processes of form $l_i \to l_k \bar{l}_j l_l$ to realize at the tree level, and it imparts one of the most stringent constraints on the model that precludes simultaneous explanation of AMMs, reducing the flavor structure down to just two textures of eq. (6.1). The partial rates for such trilepton decays are obtained in the limit when the masses of the decay products are neglected. The decay rate can be read as [16]:

$$\Gamma = \frac{1}{6144\pi^3}\frac{m_i^5}{4m_\phi^4}\left(\frac{1}{(1+\delta_{lk})}\left(\left|Y_{ik}^* Y_{jl}^*\right|^2 + \left|Y_{ki} Y_{lj}\right|^2\right) + \left|Y_{ik}^* Y_{lj}\right|^2 + \left|Y_{ki} Y_{jl}^*\right|^2\right). \tag{5.4}$$

δ_{lk} is the symmetry factor that takes care of identical particles in the final state. This expression is relevant for both $\mathcal{CP}$-even and $\mathcal{CP}$-odd neutral scalar mediated decays. Using the total muon and tau decay widths, $\Gamma_\mu^{\text{tot}} = 3.00 \times 10^{-19}\,\text{GeV}$ and $\Gamma_\tau^{\text{tot}} = 2.27 \times 10^{-12}\,\text{GeV}$,

JHEP03(2022)183

Process	Exp. Bound [1, 192]	Constraints
$\mu^- \to e^- e^+ e^-$	BR $< 1.0\times10^{-12}$ [193]	$\lvert Y_{ee}\rvert^2(\lvert Y_{e\mu}\rvert^2+\lvert Y_{\mu e}\rvert^2) < 1.16\times10^{-12}\left(\frac{m_\phi}{100\text{ GeV}}\right)^4$
$\tau^- \to e^- e^+ e^-$	BR $< 2.7\times10^{-8}$ [194]	$\lvert Y_{ee}\rvert^2(Y_{e\tau}\rvert^2+\lvert Y_{\tau e}\rvert^2) < 1.76\times10^{-7}\left(\frac{m_\phi}{100\text{ GeV}}\right)^4$
$\tau^- \to \mu^- e^+ e^-$	BR $< 1.8\times10^{-8}$ [194]	$\lvert Y_{ee}\rvert^2(Y_{\mu\tau}\rvert^2+\lvert Y_{\tau\mu}\rvert^2) < 8.78\times10^{-8}\left(\frac{m_\phi}{100\text{ GeV}}\right)^4$
$\tau^- \to \mu^- \mu^+ \mu^-$	BR $< 2.1\times10^{-8}$ [194]	$\lvert Y_{\mu\mu}\rvert^2(\lvert Y_{\mu\tau}\rvert^2+\lvert Y_{\tau\mu}\rvert^2) < 1.37\times10^{-7}\left(\frac{m_\phi}{100\text{ GeV}}\right)^4$
$\tau^- \to e^- \mu^+ \mu^-$	BR $< 2.7\times10^{-8}$ [194]	$\lvert Y_{\mu\mu}\rvert^2(\lvert Y_{e\tau}\rvert^2+\lvert Y_{\tau e}\rvert^2) < 1.32\times10^{-7}\left(\frac{m_\phi}{100\text{ GeV}}\right)^4$
$\tau^- \to e^- \mu^+ e^-$	BR $< 1.5\times10^{-8}$ [194]	$\lvert Y_{e\mu}\rvert^2(\lvert Y_{e\tau}\rvert^2+2\lvert Y_{\tau e}\rvert^2)+(\mu\leftrightarrow e) < 2.93\times10^{-7}\left(\frac{m_\phi}{100\text{ GeV}}\right)^4$
$\tau^- \to \mu^- e^+ \mu^-$	BR $< 1.7\times10^{-8}$ [194]	$\lvert Y_{e\mu}\rvert^2(\lvert Y_{\tau\mu}\rvert^2+2\lvert Y_{\mu\tau}\rvert^2)+(\mu\leftrightarrow e) < 3.32\times10^{-7}\left(\frac{m_\phi}{100\text{ GeV}}\right)^4$

Table 3. Constraints on Yukawa couplings as a function of neutral scalar mass from trilepton decays $l_i \to l_k \bar{l}_j l_l$ of charged leptons. Slightly weaker constraints on tau lepton decays from BABAR, ATLAS and LHC can be found in refs. [195–197], respectively.

we calculate the branching ratios for various processes and summarize the constraints on the Yukawa couplings as a function of the neutral scalar masses in table 3.

5.3 T-parameter constraints

The oblique parameters S, T, and U quantify the deviation of a new physics model from the SM through radiative corrections arising from shifts in gauge boson self energies [198–200]. Out of these observables, the T-parameter imposes the most stringent constraint. In the decoupling limit $\tilde{\alpha} = 0$, T-parameter in the Zee Model can be written as [201]

$$\begin{aligned} T = \frac{1}{16\pi^2\alpha_{em}\nu^2}\Big\{ & \cos^2\varphi\left[\mathcal{F}\left(m^2_{h^+},m^2_H\right)+\mathcal{F}\left(m^2_{h^+},m^2_A\right)\right]-\mathcal{F}\left(m^2_H,m^2_A\right) \\ & +\sin^2\varphi\left[\mathcal{F}\left(m^2_{H^+},m^2_H\right)+\mathcal{F}\left(m^2_{H^+},m^2_A\right)\right]-2\sin^2\varphi\cos^2\varphi\mathcal{F}\left(m^2_{h^+},m^2_{H^+}\right)\Big\} \end{aligned} \tag{5.5}$$

where,

$$\mathcal{F}\left(m_1^2,m_2^2\right) = \mathcal{F}\left(m_2^2,m_1^2\right) \equiv \frac{1}{2}\left(m_1^2+m_2^2\right) - \frac{m_1^2 m_2^2}{m_1^2-m_2^2}\log\left(\frac{m_1^2}{m_2^2}\right). \tag{5.6}$$

The allowed regions of scalar masses m_A and m_H for the choice of mixing angle between charged scalars $\sin\varphi = 0.1$ under the alignment limit are shown in figure 5, where the green and blue regions are excluded at 1σ and 2σ from T$= 0.03 \pm 0.12$ [1]. Here we fix the charged scalar mass heavier than neutral scalar mass by choosing $m_{h^+} = m_H + 200\,\text{GeV}$ and $m_{H^+} = m_H + 200\,\text{GeV}$ such that collider constraints on light charged scalars are easily satisfied [17]. Notice that the choice of φ is arbitrary and can be made small. Such a choice only makes the overall scale of neutrino mass smaller and does not alter the phenomenology for Δa_ℓ and NSI, as both can be incorporated with just the second Higgs doublet.

5.4 Muonium-antimuonium oscillations

The nontrivial mixing between bound states of muonium ($M : e^-\mu^+$) and antimuonium $\bar{M} : e^+\mu^-$ implies a non-vanishing LFV amplitude for $e^-\mu^+ \to e^+\mu^-$ [202–209]. These oscillation probabilities were measured by the PSI Collaboration, with $P(M \leftrightarrow \bar{M}) < 8.3\times10^{-11}$ at 95% C.L. [203], while MACE Collaboration at CSNS attempts to improve the

JHEP03(2022)183

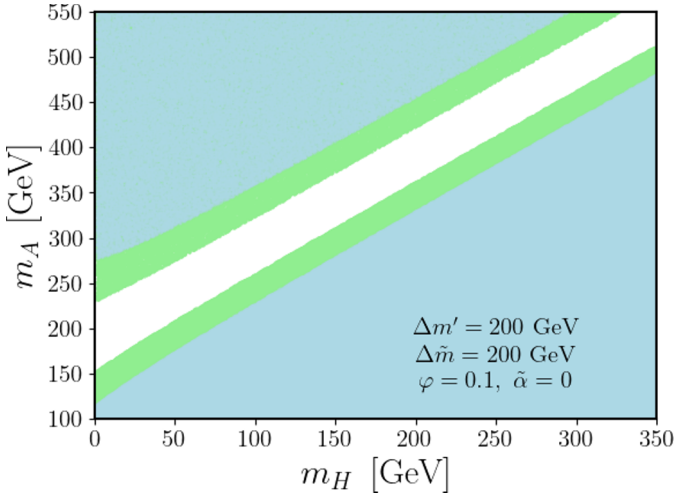

Figure 5. Allowed regions of scalar boson masses from T-parameter constraint. The green and blue regions are 1σ and 2σ exclusion from T$= 0.03 \pm 0.12$ [1], with $\Delta\tilde{m} = m_{h^+} - m_H$ and $\Delta m' = m_{H^+} - m_H$.

sensitivity at the level of $\mathcal{O}(10^{-13})$ [210]. These oscillations place a stringent constraint on the product of Yukawa couplings $Y_{e\mu}$ and $Y_{\mu e}$, thereby excluding a significant portion of parameter space as shown in figure 13 of TX-II. The muonium-antimuonium oscillation probability is given by [211, 212]

$$P(M \to \bar{M}) = \frac{64\alpha^6 m_{\rm red}^6 \tau_\mu^2}{\pi^2} G_{M\bar{M}}^2 \simeq 1.95 \times 10^5\ G_{M\bar{M}}^2 \tag{5.7}$$

where, $m_{\rm red} = m_e m_\mu/(m_e + m_\mu)$ is the reduced mass between a muon and an electron, α is the QED fine structure constant, and τ_μ is muon lifetime. $G_{M\bar{M}}$ is the Wilson coefficient [213, 214] associated with the dimension-six four fermion operator in the effective Hamiltonian density

$$\mathcal{H}_{\rm eff} = \frac{G_{M\bar{M}}}{\sqrt{2}}\ [\bar{\mu}\gamma_\mu(1+\gamma_5)e][\bar{\mu}\gamma^\mu(1-\gamma_5)e]\,. \tag{5.8}$$

From eq. (5.7), one can obtain a limit on the Wilson coefficient from PSI as $G_{M\bar{M}} \leq 1.77 \times 10^{-3}$, which translates to the bound on the Yukawa couplings as $Y_{e\mu}Y_{\mu e} \leq 2.37 \times 10^{-7}(m_H/\text{GeV})^2$. Similarly, the bound from the MACE experiment is expected to improve the sensitivity by at least two orders $\mathcal{O}(10^{-13})$ which corresponds to $Y_{e\mu}Y_{\mu e} \leq 8.11 \times 10^{-9}(m_H/\text{GeV})^2$.

5.5 Direct experimental constraints

In this section, we analyze various direct experimental constraints on the neutral scalar with mass in the range of 100 MeV to 300 GeV range that explains Δa_ℓ. There are various experimental constraints one needs to consider, such as dark photon searches, rare Z-decay constraints, and LEP and LHC constraints. The lack of observation of dark photon A_d in searches through the $e^+e^- \to \gamma A_d$, with $A_d \to e^+e^-$ channel at KLOE [215, 216] and

JHEP03(2022)183

BaBar [217, 218] sets strong constraints on the couplings. By recasting the results from BaBar and KLOE, one can put a bound on the mass of the light scalars and the corresponding Yukawa couplings, as depicted by the brown and blue shaded region in figure 12. Similarly, for the scalar mass $m_H > 200\,\text{MeV}$, the dark-boson searches at the BaBar [187] can be recast to limit on mass and the Yukawa couplings via the process $e^+e^- \to \mu^+\mu^- H$ [219, 220], shown as the pink shaded region in figure 12. We observe that the searches at BaBar exclude $Y_{\mu\mu} \gtrsim 6 \times 10^{-3}$ (1.5×10^{-2}) at $m_H = 0.212\,\text{GeV}$ (10 GeV). In the relatively heavier mass regime, $m_H \gtrsim \mathcal{O}(10)\,\text{GeV}$, $Y_{\mu\mu}$ is constrained by LHC search limits. For example, direct Z' searches at the LHC in the $pp \to \mu^+\mu^-(Z' \to \mu^+\mu^-)$ channel leads to upper limits on the production cross-section times branching ratio [188]. These upper limits could, in turn, be recast to upper bounds on the Yukawa couplings of our interest. We illustrate its implication on our parameter space as a purple shaded region in the $\{Y_{\mu\mu}, m_H\}$ plane in figure 12 (left panel).

The Yukawa couplings of the leptophilic Higgs boson H are also susceptible to constraints from searches at the LEP. Direct searches in contact interaction processes $e^+e^- \to \ell^+\ell^-$ ($\ell = e, \mu$) and Higgs production in association with leptons $e^+e^- \to \ell^+\ell^-(H \to \ell^+\ell^-)$ can potentially constrain the Yukawa couplings in both `TX-I` and `TX-II`. In the heavy mass limit, LEP data exclude an effective cutoff scale $\Lambda \simeq m_H/Y_{ij}$ [221]. The LEP contact interaction constraints on Λ for a light neutral scalar H are no longer applicable. However, due to the t-channel contribution of H/A that interferes with the SM process, the cross-section of $e^+e^- \to \ell^+_\alpha \ell^-_\alpha$ can still be modified. By implementing the model file in the `FeynRules` package [222], we computed the cross-sections using `MadGraph5_aMC@NLO` [223], which are then compared with the measured cross-sections [221, 224] to get a limit on Yukawa coupling as a function of scalar mass; $Y_{ee} < 0.8$ and $Y_{e\mu} < 0.74$ for the benchmark value of $m_H = 130\,\text{GeV}$ [17]. This limit is slightly weaker than the bounds from searches in the $e^+e^- \to \ell^+\ell^-(H \to \ell^+\ell^-)$ channel, discussed later in great detail.

The most constraining Higgs production processes for Y_{ee} and $Y_{e\mu}$ are $e^+e^- \to e^+e^-$ ($H \to e^+e^-$) and $e^+\mu^-(H \to e^+\mu^-)$, respectively. Likewise, $Y_{\mu\mu}$ would be most sensitive to the $e^+e^- \to \mu^+\mu^-(H \to \mu^+\mu^-)$ process. However, the production cross-section of the latter at LEP is roughly an order of magnitude smaller than its former two counterparts. Therefore, we ignore the constraints on $Y_{\mu\mu}$ from direct searches in the $e^+e^- \to \mu^+\mu^-(H \to \mu^+\mu^-)$ channel for the present analysis. In order to correctly estimate the LEP bounds on Y_{ee} ($Y_{e\mu}$), we generate signal events in the $e^+e^- \to e^+e^-(H \to e^+e^-)$ ($e^+e^- \to e^+\mu^-(H \to e^+\mu^-)$) channel assuming $\sqrt{s} = 207\,\text{GeV}$ for several values of m_H at the leading order (LO) using the `MadGraph5_aMC@NLO` [223] package. We also simulate the respective dominant background processes: $4e$ ($2e2\mu$) in the same framework. We reconstruct the Higgs boson by identifying the e^+e^- ($e^+\mu^-$) pair with the smallest $\Delta R = \sqrt{\Delta\eta^2 + \Delta\phi^2}$ separation, where $\Delta\phi$ is the azimuthal angle difference between the opposite sign lepton pairs. Consequently, we compute the signal and background efficiencies and translate them into upper bounds on Y_{ee} ($Y_{e\mu}$) as a function of m_H. We illustrate the current upper limits from LEP on Y_{ee} and $Y_{e\mu}$ as grey shaded regions in the right panel of figure 12 and figure 13, respectively. We would like to note that we do not include any LEP detector effects in these studies, and therefore our "LEP estimations" must be treated cautiously. As such, these upper limits are rather conservative estimations.

JHEP03(2022)183

In principle, the Higgs boson could have been reconstructed by identifying the opposite sign lepton pairs with invariant mass closest to m_H. However, such a reconstruction strategy leads to an almost 100% signal efficiency for all choices of m_H since we are restricted to a simplistic truth level analysis without accounting for detector effects. This could potentially entail considerably stronger upper limits on the Yukawa couplings than a realistic scenario leading to misleading implications. We note that we have adopted this reconstruction strategy in section 7, where we perform a detailed cut-based collider analysis at the detector level to study the future sensitivity on Y_{ee}, $Y_{e\mu}$ and $Y_{\mu\mu}$ from future lepton colliders.

For completeness, we would like to note that the charged scalar in the model can be pair produced directly at colliders via s-channel off-shell photon or Z exchange with $H^\pm$ further decaying into $\ell\nu$. The corresponding LEP bound is $m_{H^\pm} \gtrsim 80\,\text{GeV}$ [225] for $\tau\nu$ final state. Moreover, these leptonic final states $\ell\nu$ mimic slepton searches in supersymmetric models that can be recast for our scenario and provide a lower bound on its mass $m_{H^\pm} \gtrsim 100\,\text{GeV}$ [17]. Similarly at the LHC, the s-channel Drell-Yan process $pp \to \gamma^*/Z^* \to H^+H^-$ provides a somewhat stronger limit of $m_{H^\pm} \gtrsim 200\,\text{GeV}$ [17] for $\text{BR}(H^\pm \to e\nu) = 1$. Note that the LHC limits can be evaded by lowering the branching ratio, which can be always be done with more than one Yukawa coupling.

6 Flavor structures

This section explores the texture of the Yukawa coupling matrix Y for a unified explanation of electron and muon $g-2$ while correctly reproducing neutrino oscillation data. The Yukawa coupling f appearing in the neutrino mass formula given in eq. (2.7) is taken to be arbitrary and small such that it automatically satisfies all the constraints and generates the correct order of the neutrino masses. However, the Yukawa matrix Y has non-trivial structures and its various components explain $\Delta a_{e/\mu}$ as previously discussed in section 3, for instance, eq. (3.8) for one-loop texture. It turns out that the Yukawa couplings $Y_{ie}(i = e, \mu, \tau)$, which is a part of the texture to explain Δa_ℓ, also induce NSI at some level. A cursory glance at the analysis of LFV processes in section 5 reveals two types of Yukawa textures to accommodate both AMMs in conjunction with neutrino observables, which are:

$$\textbf{TX-I:}\quad Y = \begin{pmatrix} Y_{ee} & 0 & 0 \\ 0 & Y_{\mu\mu} & \times \\ 0 & \times & Y_{\tau\tau} \end{pmatrix}, \qquad \textbf{TX-II:}\quad Y = \begin{pmatrix} 0 & Y_{e\mu} & 0 \\ Y_{\mu e} & 0 & \times \\ 0 & \times & \times \end{pmatrix}. \tag{6.1}$$

These textures are studied in detail in section 8. Here the green, blue, and red color-coded entries respectively represent Δa_μ, Δa_e, and NSI. The same couplings that can explain more than one observables are encircled with the corresponding colors. The $\times$'s denote the Yukawa couplings required to satisfy the five neutrino oscillation observables $(\Delta m^2_{21}, \Delta m^2_{31}, \sin^2\theta_{13}, \sin^2\theta_{23}, \sin^2\theta_{12})$ while satisfying the flavor constraints such as $\ell_i \to \ell_j\gamma$ and trilepton decay (cf. section 5). For more details, see section 8. We also note that the zeros in the matrices of eq. (6.1) need not be exactly zero, but they need to be sufficiently small so that the flavor-changing processes remain under control (cf. section 5). Note that

JHEP03(2022)183

the flavor structures are proposed under the assumption that m_H is smaller than all other new scalar bosons.

TX-I. Here, we examine the texture where both Δa_e and Δa_μ could be explained from the diagonal Yukawa couplings Y_{ii}. For the choice of real Yukawa couplings, $Y_{\mu\mu}$ can explain Δa_μ at one-loop order parametrized by the chirally enhanced term of eq. (3.2). The one-loop contribution from Y_{ee} alone always gives the wrong sign to Δa_e. However, the inclusion of a third Yukawa coupling $Y_{\tau\tau}$, appearing from the two-loop Barr-Zee diagram, can generate the correct sign for Δa_e [141]. Furthermore, the same Yukawa coupling Y_{ee} induces NSI, as previously discussed in section 4. On the other hand, for complex Yukawa couplings, concurrent solutions do exist, for instance, $Y_{\mu\mu} \in \mathbb{R} \cap Y_{ee} \in \mathbb{I}$ for $m_A > m_H$ and vice versa for $m_A < m_H$. Note that any nonzero phase in the Yukawa couplings would be constrained by EDMs (cf. section 3.1).

TX-II. The only other flavor structure to incorporate Δa_e and Δa_μ while satisfying neutrino oscillation data is given in eq. (6.1) as `TX-II` with Yukawa couplings $Y_{e\mu}$ and $Y_{\mu e}$. With non-zero $Y_{e\mu}(e \leftrightarrow \mu)$, the diagonal couplings $Y_{ii}(i = e, \mu)$ are highly constrained from $\mu \to e\gamma$ (cf. section 5.1). Thus, the two-loop contributions are highly suppressed and can be safely ignored. To explain both the anomalies, $Y_{e\mu}$ and $Y_{\mu e}$ can take opposite signs to get Δa_e negative. Moreover, considering a hierarchy among the two Yukawa couplings, one can explain Δa_μ from the non-chiral part of eq. (3.2). Details on the choice of the Yukawa couplings as a function of the mass of scalar field is given in figure 13 in section 8. Note that $Y_{\mu e} \sim \mathcal{O}(1)$ can induce NSI. However, such a choice necessarily requires $|Y_{\mu e}| > |Y_{e\mu}|$ to get the correct order for Δa_ℓ, which turns out to be not in favor with the normal hierarchy (NH) solution to the neutrino oscillation data (cf. section 8).

For the sake of completeness, we also point out that $Y_{\tau e}$ can induce large NSI, $\epsilon_{\tau\tau} \sim 9.3\%$ [17], and provide correction to a_e from tau mass chiral enhancement involving the coupling $Y_{e\tau}$. As was the case before, the Δa_e emerges from one-loop diagrams alone. However, there exists no choice of Yukawa couplings that can incorporate Δa_μ in this scenario; LFV processes highly suppress all the couplings that provide corrections a_μ.

7 Collider analysis

The Yukawa structure of the new Higgs boson H required to simultaneously explain Δa_ℓ, NSI as well as neutrino oscillation data entails concurrent non-zero values of all three diagonal elements $\{Y_{ee}, Y_{\mu\mu}, Y_{\tau\tau}\}$ or the first and second generation off-diagonal entries $\{Y_{e\mu}, Y_{\mu e}\}$, as discussed in section 6. At lepton colliders, these couplings could be directly accessed via searches in the $e^+e^- \to \ell^+\ell^- \, (H \to \ell^+\ell^-)$ channel, where $\ell = e, \mu$. In this section, we explore the sensitivity of the aforesaid channels to probe Y_{ee} and $Y_{e\mu}$ at the projected ILC configuration: $\sqrt{s} = 1$ TeV with an integrated luminosity $\mathcal{L} = 500$ fb^{-1} [151–155]. We also study the projected sensitivity on $Y_{\mu\mu}$ from direct searches in the $\mu^+\mu^- \to \mu^+\mu^- \, (H_2 \to \mu^+\mu^-)$ channel at the future muon collider (MuC) with configuration: $\sqrt{s} = 3$ TeV, $\mathcal{L} = 1$ ab^{-1} [156, 157].

JHEP03(2022)183

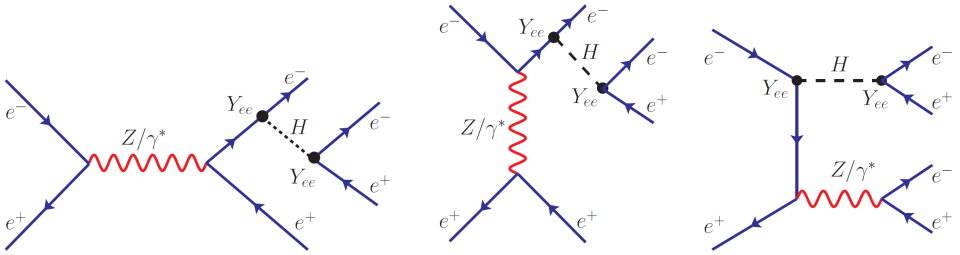

Figure 6. Some illustrative LO Feynman diagrams for the signal process: $e^+e^- \to e^+e^-$ $(H_2 \to e^+e^-)$.

We generate signal and background events at leading order (LO) using the `MadGraph5_aMC@NLO` [223] framework. Showering and hadronization is performed with `Pythia-8` [226, 227] while fast detector response is simulated with `Delphes-3.5.0` [228]. We utilize the default `ILCgen` [229] and `MuonCollider` [230] detector cards to simulate the response of the ILC and the muon collider.

7.1 Y_{ee} at ILC

We study the projected sensitivity on Y_{ee} at the ILC using the channel

$$e^+e^- \to e^+e^-H \to e^+e^-\left(H \to e^+e^-\right). \tag{7.1}$$

A few typical leading order (LO) Feynman diagrams of this process are illustrated in figure 6. The dominant SM background is $e^+e^- \to e^+e^-e^+e^-$.

We select events containing exactly two isolated electrons and two isolated positrons in the final state with $p_T > 2\,\text{GeV}$ and $|\eta| < 3.0$. We further impose $p_{T,e_{1,2}} > 10\,\text{GeV}$ and $p_{T,e_{3,4}} > 5\,\text{GeV}$, where e_1 and e_4 are the highest and lowest p_T leptons, respectively. In figure 7, we illustrate the p_T distribution of the highest and second-highest p_T leptons, e_1 and e_2, respectively, for three signal benchmarks, $M_H = 10$, 130 and 230 GeV, and the $4e$ background process. In the signal process, the Higgs boson can recoil against an electron or a positron as seen in the first two diagrams in figure 6. This leads to an overall improvement in the p_T of the recoiling electron with increasing M_H. At relatively large m_H, this recoiling electron becomes the dominant constituent in e_1. Correspondingly, we expect to see an upward shift in the peak of p_{T,e_1} distribution with increasing m_H. We observe this behaviour in figure 7 where p_{T,e_1} peaks at $\sim 60\,\text{GeV}$ in the $M_H = 10\,\text{GeV}$ scenario and the peak position shifts to $p_{T,e_1} \sim 90$ and $\sim 130\,\text{GeV}$ in the $m_H = 130$ and 230 GeV scenarios, respectively. Furthermore, we observe that the overall distribution gets flatter with increasing m_H. The background p_T distribution of e_1 and e_2 peaks at $s \sim 90$ and ~ 60 GeV, respectively, which roughly coincides with the peak in the $M_H = 130\,\text{GeV}$ scenario. The $4e$ background process also includes diagrams where an on-shell Z boson recoils against an electron or positron leading to the aforesaid similarity in peak positions. Next, let us focus on the pseudorapidity distributions of the final state leptons. We present the η_{e_1} and η_{e_2} distributions in figure 7. We observe that e_1 and e_2 in the background are mostly produced in the forwards regions of the detector due to back-to-back production

JHEP03(2022)183

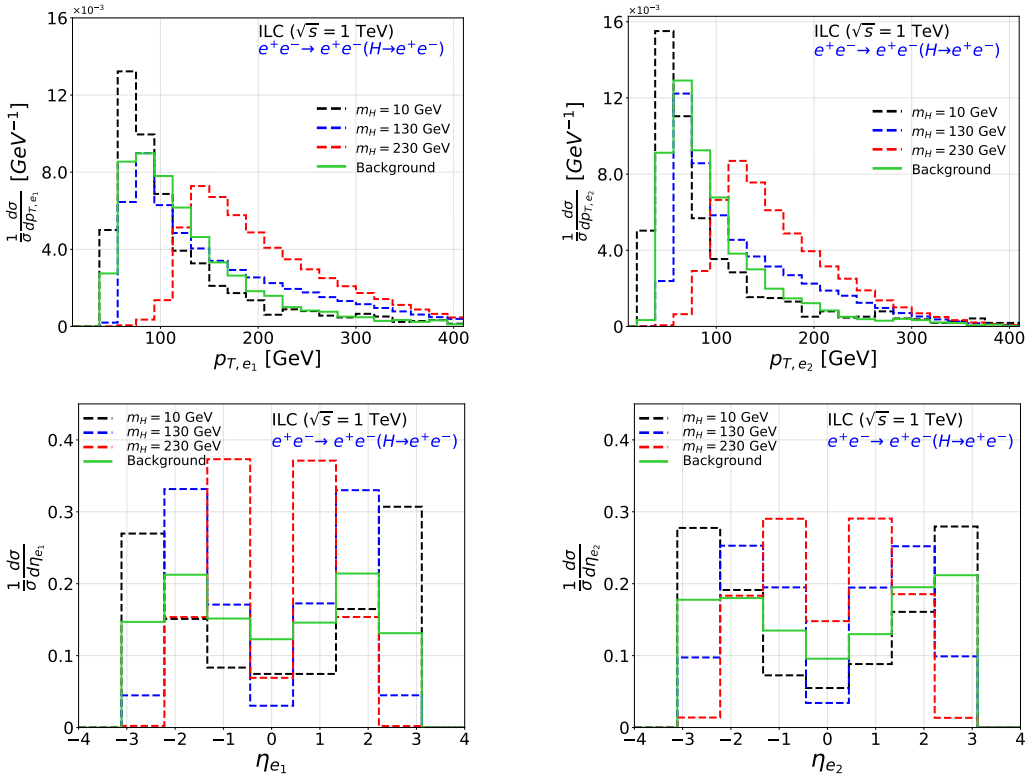

Figure 7. p_T and η distributions of the final state electrons with the highest and 2^{nd} highest p_T, e_1 and e_2, respectively, in the $e^+e^- \to e^+e^-(H \to e^+e^-)$ channel at the ILC with $\sqrt{s} = 1$ TeV. The black, blue and red dashed lines represent the distributions for signal benchmarks $m_H = 10$, 130 and 230 GeV, respectively. The background distribution is presented as green solid line.

of electron-positron pairs. On the contrary, the leading and sub-leading p_T leptons in signal benchmarks with large m_H (~ 230 GeV) are mostly produced in the central regions $|\eta| \lesssim 1.0$ by virtue of their larger transverse momenta. At relatively smaller Higgs masses $M_H \sim 10$ and 130 GeV, the peaks in pseudorapidity distribution roughly coincides with that of background.

The four final state leptons can be classified into four opposite sign (OS) lepton pairs, one of which is produced from the decay of H in the signal process. The electron-positron pair associated with H is identified by minimizing $(m^2_{e^+e^-} - m^2_H)$, where $m_{e^+e^-}$ is the invariant mass of an OS electron pair and m_H is the mass of H in the signal benchmark under consideration. We present the invariant mass distribution of the reconstructed Higgs boson $H_{\rm rec}$ in figure 8 for three signal benchmark scenarios $m_H = 10,\ 130$ and 230 GeV as dashed black, blue and red lines, respectively. The respective background distributions are presented in solid lines.

Taking cognizance of the $m_{H_{\rm rec}}$ distributions in figure 8, we require signal and background events to satisfy $m_H \pm 10$ GeV. In addition, we also optimize the selection cuts on p_{T,e_1},η_{e_1} and η_{e_2} for several signal benchmarks in order to maximize the signal significance $\sigma_S = S/\sqrt{S+B}$, where S and B are the signal and background yields. In table 4, we

JHEP03(2022)183

m_H [GeV]	Optimized cuts			Signal eff.	Bkg eff.
	$P_{T,e_1} >$ [GeV]	$\lvert\eta_{e_1}\rvert <$	$\lvert\eta_{e_2}\rvert <$		
10	40	3.0	3.0	0.002	0.004
40	30	2.7	2.7	0.066	0.005
70	30	3.0	3.0	0.207	0.007
100	40	2.6	2.9	0.328	0.010
130	60	2.4	2.5	0.385	0.003
160	70	2.1	2.3	0.415	0.002
190	90	2.0	2.2	0.455	0.002
230	110	1.7	2.0	0.457	0.001
270	140	1.6	1.9	0.475	9×10^{-4}
310	150	1.6	2.2	0.511	8×10^{-4}
350	180	1.3	2.5	0.476	5×10^{-4}

Table 4. Optimized selection cuts on p_{T,e_1}, η_{e_1} and η_{e_2}, signal efficiency and background efficiency, from cut-based analysis in the $e^+e^- \to e^+e^-(H \to e^+e^-)$ channel at $\sqrt{s} = 1$ TeV ILC for several signal benchmark points.

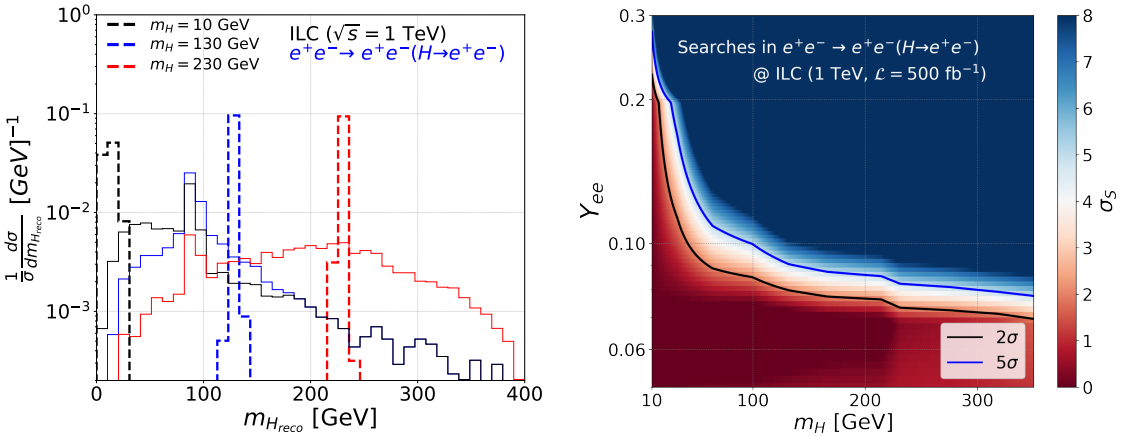

Figure 8. *Left:* invariant mass distribution of the reconstructed Higgs boson for three signal benchmarks $m_H = 10$ (black dashed), 130 (blue dashed) and 230 GeV (red dashed). The corresponding solid lines represent the respective $4e$ background distributions. *Right:* projected upper limits on Y_{ee} from direct searches in the $e^+e^- \to e^+e^-$ $(H \to e^+e^-)$ channel at the 1 TeV ILC assuming $\mathcal{L} = 500\,\text{fb}^{-1}$. The black solid and blue solid lines represent the projected upper limits at 2σ and 5σ, respectively. The color palette in the z-axis represents the signal significance.

present the optimized selection cuts, signal and background yields, along with the signal significance, for several signal benchmarks within the range 10 GeV $\leq M_H \leq$ 350 GeV. We utilize the optimized signal and background efficiencies obtained in the previous step to derive the projected sensitivity on Y_{ee} as a function of M_H at the ILC 1 TeV machine. We present our results as upper limit projections at 2σ and 5σ in the $\{Y_{ee}, M_H\}$ plane in figure 8.

JHEP03(2022)183

We observe that the projected upper limits are weaker at small $m_H \sim 10$ GeV, and improves by a factor of ~ 3 until $m_H \sim 50\,\text{GeV}$. Afterwards, it gradually improves with increasing m_H. At a particular $\{Y_{ee}, m_H\}$, the projected sensitivity is determined by three factors: the signal production cross-section $\propto Y_{ee}$ and m_H, signal efficiency $\propto m_H$ and background efficiency. At the ILC 1 TeV run, the LO production cross-section of the signal process in eq. (7.1), $\sigma_{Y_{ee}}$, peaks at roughly ~ 100 fb with $m_H \sim 220$–240 GeV for $Y_{ee} = 1.0$, and falls down to ~ 7 fb (~ 70 fb) at $m_H \sim 10\,\text{GeV}$ (350 GeV), respectively. On the other hand, we observe that the signal efficiency in table 4 improves with increasing m_H until around 310 GeV after which it falls down marginally at $m_H = 350\,\text{GeV}$. The signal efficiency improves by $\mathcal{O}(100)$ from ~ 0.002 at $m_H = 10\,\text{GeV}$ to around 0.207 at $m_H = 70\,\text{GeV}$. Afterwards, it registers a gradual rise to ~ 0.511 at $m_H = 310\,\text{GeV}$. At $m_H = 350\,\text{GeV}$, it falls down to 0.476. The background efficiency, on the other hand, exhibits maximal value near $m_H \sim m_Z$. It improves from ~ 0.004 at $m_H = 10\,\text{GeV}$ to ~ 0.01 at $m_H = 100\,\text{GeV}$ beyond which it gradually falls down by a factor of ~ 20 to $\sim 5 \times 10^{-4}$ at $m_H = 350\,\text{GeV}$. At small m_H ($\lesssim 70\,\text{GeV}$), the small signal production cross-section coupled with a relatively small signal efficiency leads to weaker sensitivity on Y_{ee}. In the $70\ \text{GeV} \lesssim m_H \lesssim 230\,\text{GeV}$ region, both signal production cross-section and efficiency improves while the background efficiency deteriorates. All these factors contribute towards improving the projected sensitivity. As we move to signal benchmarks with heavier m_H, the signal production cross-section registers a decrement. However, the signal efficiency continues to increase until $m_H = 310\,\text{GeV}$ and the background efficiency continues to plummet. The later two counters the decrements in signal cross-section, and the projected upper limits continue improving. At $m_H = 350\,\text{GeV}$, the signal efficiency is $\mathcal{O}(8\%)$ smaller than its $m_H = 310\,\text{GeV}$ counterpart. However, this decrement in signal efficiency is not reflected in the projected upper limits in figure 8 since the background efficiency falls down by a relatively larger rate $\mathcal{O}(40\%)$. Overall we observe that the 1 TeV ILC machine would be able to probe Y_{ee} up to $Y_{ee} \gtrsim 0.085$ (at 2σ) at $m_H = 100\,\text{GeV}$ via direct searches in the $e^+e^- \to e^+e^-(H \to e^+e^-)$ channel.

7.2 $Y_{e\mu}$ at ILC

To explore the projected sensitivity to $Y_{e\mu}$, we consider the channel

$$e^+e^- \to e^\pm\mu^\mp H \to e^\pm\mu^\mp(H \to e^\pm\mu^\mp). \tag{7.2}$$

We consider events containing an OS electron pair and an OS muon pair. All four leptons ($\ell = e, \mu$) are required to have $p_T > 2\,\text{GeV}$ and $|\eta| < 3.0$. The leptons are also required to satisfy $p_{T_{\ell_{1,2}}} > 10\,\text{GeV}$ and $p_{T_{\ell_{3,4}}} > 5\,\text{GeV}$, where ℓ_1 and ℓ_4 are the highest and lowest p_T leptons, respectively. The kinematic behavior of the final state leptons are similar to that exhibited in the $e^+e^- \to e^+e^-(H \to e^+e^-)$ channel. One major difference however is the absence of t-channel electron exchange diagrams, shown in the right panel of figure 6, since the H couples to $e^\pm\mu^\mp$ pair instead of e^+e^- pair. In figure 9, we present the p_T and η distributions of l_1 and l_2 for three signal benchmarks $m_H = 10,\ 130$ and $240\,\text{GeV}$, and the $2e2\mu$ background. We observe that the overall features are roughly similar to that

JHEP03(2022)183

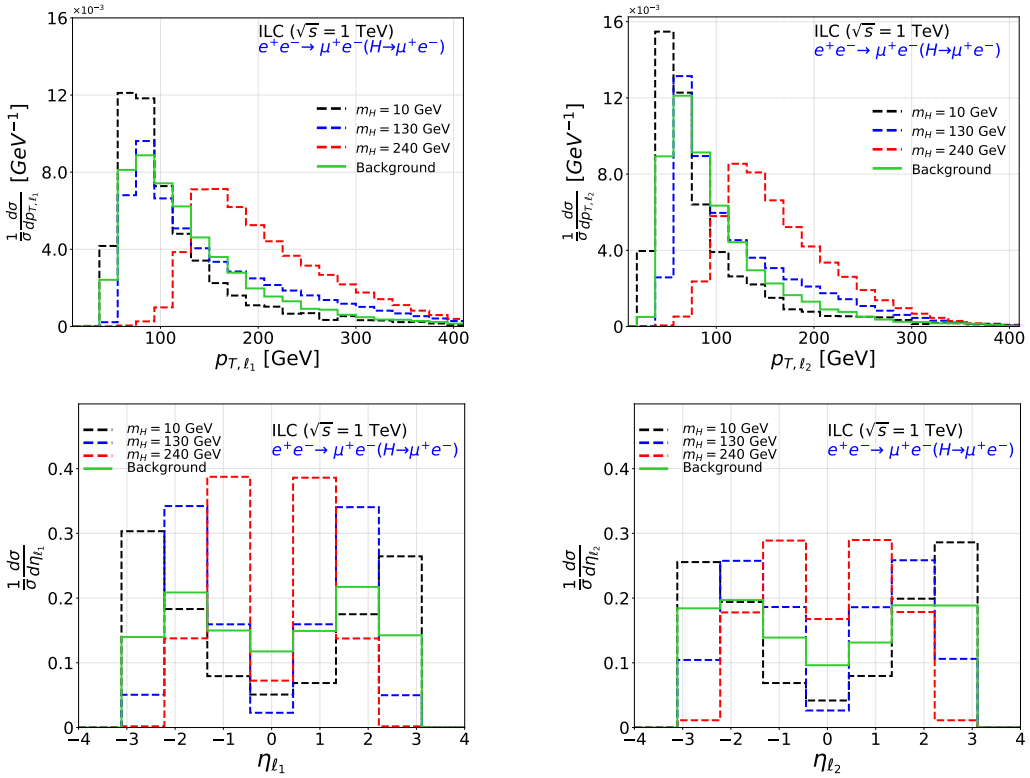

Figure 9. p_T and η distributions of the final state leptons with the highest and 2^{nd} highest p_T, ℓ_1 and ℓ_2, respectively, in the $e^+e^- \to \mu^+e^-(H \to \mu^+e^-)$ channel at the ILC with $\sqrt{s} = 1\,\text{TeV}$. The black, blue and red dashed lines represent the distributions for signal benchmarks $m_H = 10$, 130 and 240 GeV, respectively. The background distribution is presented as green solid line.

in section 7.1. Here as well, the peak of the p_T distributions shifts to larger values with increasing m_H. Similarly, the relative concentration of ℓ_1 and ℓ_2 in the central regions of the detector improves with m_H.

In order to reconstruct the Higgs boson, we perform mass minimization similar to that in section 7.1. We associate an OS electron-muon pair with H that minimizes $(m^2_{e^\pm\mu^\mp} - m^2_H)$. In figure 10, we present the invariant mass distribution of the reconstructed Higgs boson for several signal benchmarks and the $2e2\mu$ background. We impose $|m_{H_{\text{reco}}} \pm 10\ \text{GeV}|$ to filter the signal from the $2e2\mu$ background continuum. Additionally, we also optimize selection cuts on p_{T,ℓ_1}, η_{ℓ_1} and η_{ℓ_2}. We present the optimized signal and background efficiency for several choices of m_H along with the respective set of optimized cuts in table 5. Both signal and background efficiencies follow a similar behaviour to that in section 7.1. We observe that the signal efficiency improves by a factor of ~ 40 from ~ 0.007 at $m_H = 10\,\text{GeV}$ to ~ 0.281 at $m_H = 70\,\text{GeV}$. On further increasing m_H, it reaches to ~ 0.639 at $m_H = 310\,\text{GeV}$ before falling down to ~ 0.627 at $m_H = 350\,\text{GeV}$. We translate these efficiencies into upper limit projections in $\{Y_{e\mu}, m_H\}$ plane, shown in figure 10. We observe that the 1 TeV ILC machine would be able to probe $Y_{e\mu}$ up to ~ 0.1 and ~ 0.09 at $m_H = 100$ and 200 GeV, respectively, at 2σ. We note that the projected sensitivity on $Y_{e\mu}$ is relatively weaker compared to Y_{ee} (see section 7.1) due to relatively smaller signal production cross-section in the present channel.

JHEP03(2022)183

m_H [GeV]	Optimized cuts			Signal eff.	Bkg eff.
	$P_{T,e_1} >$ [GeV]	$\lvert\eta_{e_1}\rvert <$	$\lvert\eta_{e_2}\rvert <$		
10	30	3.0	3.0	0.007	0.002
40	20	3.0	3.0	0.113	0.003
70	30	3.0	3.0	0.281	0.004
100	40	2.7	2.9	0.428	0.006
130	40	2.5	2.7	0.505	0.002
190	90	2.1	2.3	0.584	0.001
240	110	1.8	2.2	0.618	7×10^{-4}
270	130	1.7	2.1	0.625	6×10^{-4}
310	140	1.6	2.1	0.639	4×10^{-4}
350	160	1.4	2.0	0.627	3×10^{-4}

Table 5. Optimized selection cuts on p_{T,e_1}, η_{e_1} and η_{e_2}, signal efficiency and background efficiency, from cut-based analysis in the $e^+e^- \to \mu^+e^-(H \to \mu^+e^-)$ channel at $\sqrt{s} = 1$ TeV ILC for several signal benchmark points.

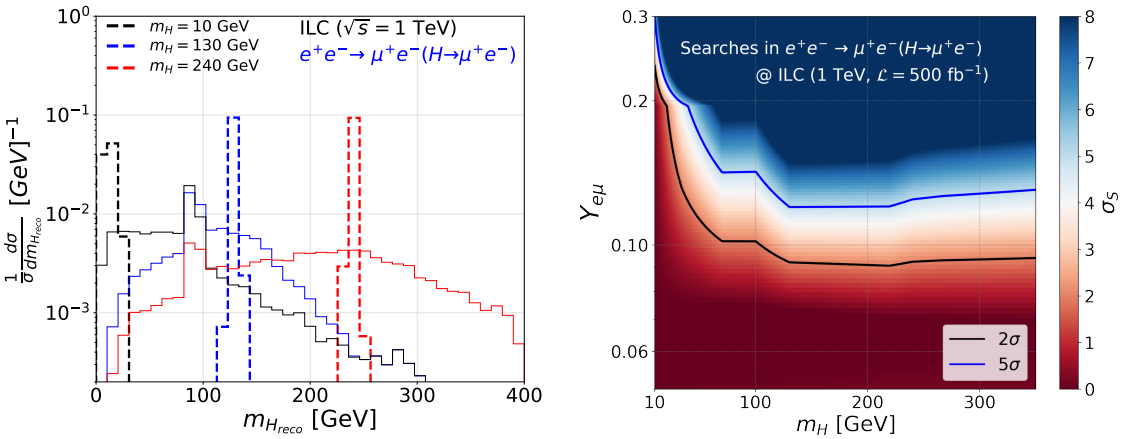

Figure 10. *Left:* invariant mass distribution of the reconstructed Higgs boson for three signal benchmarks $m_H = 10$ (black dashed), 130 (blue dashed) and 240 GeV (red dashed). The corresponding solid lines represent the respective $2e2\mu$ background distributions. *Right:* projected upper limits on $Y_{e\mu}$ from direct searches in the $e^+e^- \to \mu^+e^-$ $(H \to \mu^+e^-)$ channel at the 1 TeV ILC assuming $\mathcal{L} = 500\,\text{fb}^{-1}$. The black solid and blue solid lines represent the projected upper limits at 2σ and 5σ, respectively. The color palette in the z-axis represents the signal significance.

JHEP03(2022)183

m_H [GeV]	Signal eff.	Bkg eff.
10	0.006	0.005
40	0.151	0.005
70	0.267	0.005
100	0.291	0.022
150	0.292	0.003
200	0.297	0.003
250	0.321	0.002
300	0.369	0.002
350	0.395	0.002

Table 6. Signal and background efficiencies, from cut-based analysis in the $\mu^+\mu^- \to \mu^+\mu^-$ $(H \to \mu^+\mu^-)$ channel at $\sqrt{s} = 3\,\text{TeV}$ MuC for several signal benchmark points.

7.3 $Y_{\mu\mu}$ at future muon collider

The $e^+e^- \to \mu^+\mu^-(H \to \mu^+\mu^-)$ channel offers a direct probe to the $Y_{\mu\mu}$ coupling at electron-positron colliders. However, the production cross-section of this process is at least an order of magnitude smaller relative to $e^+e^- \to e^+e^-(H \to e^+e^-)$ process due to the absence of t-channel Z/γ^* exchange diagrams, leading to weaker sensitivity. The issue of smaller production cross-section could be, however, circumvented at a muon collider (MuC). Muons produce less synchrotron radiation relative to the electrons, and therefore, a MuC machine could be operated at a much higher center of mass energies compared to an electron-positron collider. Consequently, the most stringent sensitivity on muon Yukawa coupling via direct searches in the $\ell^+\ell^-H$ channel could perhaps be achieved at a future MuC. Taking this into consideration, in the present section, we explore the potential capability of a muon collider with configuration $\{\sqrt{s} = 3\,\text{TeV}, \mathcal{L} = 1\,\text{ab}^{-1}\}$ to probe $Y_{\mu\mu}$ via direct searches in the $\mu^+\mu^- \to \mu^+\mu^-(H \to \mu^+\mu^-)$ channel. In order to simulate detector response, we utilize the default `Delphes` card for a muon collider [230].

We require events to contain exactly four isolated muons in the final state. We assume detector coverage up to $|\eta| < 2.5$, and also impose $p_{T,\mu} > 10\,\text{GeV}$. The final state muons exhibit kinematic features that are similar to that of the final state electrons in section 7.1. Consequently, we adopt the mass minimization strategy from section 7.1 to reconstruct the Higgs boson. We do not present the $m_{H_{\text{reco}}}$ distribution in the present scenario due to its close similarity with figure 8. The dominant background source is the $\mu^+\mu^- \to 4\mu$ process. We impose additional selection cuts on the p_T of the final state muons in order to improve signal-background discrimination:

$$p_{T,\mu_1} > 90\ \text{GeV} \quad p_{T,\mu_2} > 20\ \text{GeV}, \quad p_{T,\mu_3} > 15\ \text{GeV}, \tag{7.3}$$

where, μ_1 represents the highest p_T muon.

We tabulate the signal and background efficiencies for various signal benchmarks corresponding to different values of m_H in table 6. In the Higgs mass range of our interest

JHEP03(2022)183

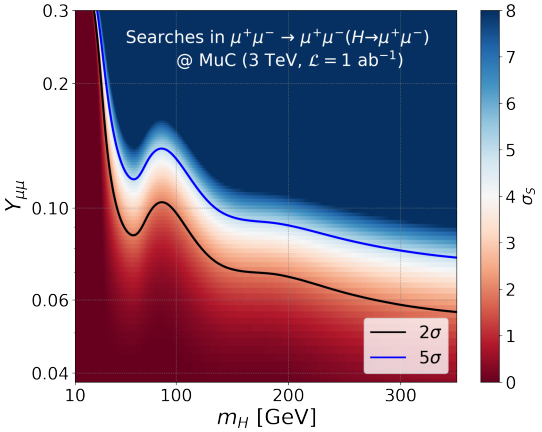

Figure 11. Projected upper limits on $Y_{\mu\mu}$ from direct searches in the $\mu^+\mu^- \to \mu^+\mu^-$ $(H \to \mu^+\mu^-)$ channel at the 3 TeV MuC assuming $\mathcal{L} = 1\,\text{ab}^{-1}$. The black solid and blue solid lines represent the projected upper limits at 2σ and 5σ, respectively. The color palette in the z-axis represents the signal significance as a function of $\{Y_{\mu\mu}, m_H\}$.

10 GeV $< m_H <$ 350 GeV, we observe that the signal efficiency improves with increasing m_H. The background efficiency, on the other hand, falls down with m_H except for m_H close to m_Z where the leptons from Z resonance fill into the $m_{H_{\text{reco}}}$ distribution. We utilize these efficiencies to derive projected upper limits on $Y_{\mu\mu}$ as a function of m_H. We illustrate the 2σ and 5σ projections in figure 11. The signal efficiency improves by more than one order of magnitude from ~ 0.006 at $m_H = 10\,\text{GeV}$ to ~ 0.151 at $m_H = 40\,\text{GeV}$, while the signal production cross-section improves by a factor of ~ 6. The background efficiency, on the other hand, remains almost unchanged. This leads to an order of magnitude improvement in the projected upper limits on $Y_{\mu\mu}$. At $m_H = 100\,\text{GeV}$, the background efficiency is roughly 4 times higher than at its neighbour signal benchmark points in table 6 due to its closeness to the Z resonance. This translates into a weakening in the projected upper limits in the vicinity of m_Z as seen in figure 11. Above m_Z, we observe that the signal efficiency continues to grow while the background efficiency keeps falling gently with increasing m_H. The signal production cross-section also continues to rise. All these factors lead to a gradual strengthening in the projected upper limits on $Y_{\mu\mu}$ with increasing m_H. At $m_H = 300\,\text{GeV}$, we observe that MuC would be able to probe $Y_{\mu\mu}$ up to ~ 0.06 at 2σ.

8 Results and discussions

In this section, we present numerical analysis for the model parameter space and reconcile electron and muon $g-2$ within their 1σ measured values while being consistent with all the low-energy, LHC, and LEP constraints discussed in the previous sections. After exhausting all the possibilities, we find two minimum textures discussed in eq. (6.1) of section 6 to incorporate both of these anomalies and have a consistent neutrino oscillation fit $(\Delta m^2_{21}, \Delta m^2_{31}, \sin^2\theta_{13}, \sin^2\theta_{23}, \sin^2\theta_{12})$. The neutrino mass matrix given in eq. (2.7) is diagonalized by a unitary transformation

$$U^T M_\nu U = \widehat{M}_\nu\,, \tag{8.1}$$

JHEP03(2022)183

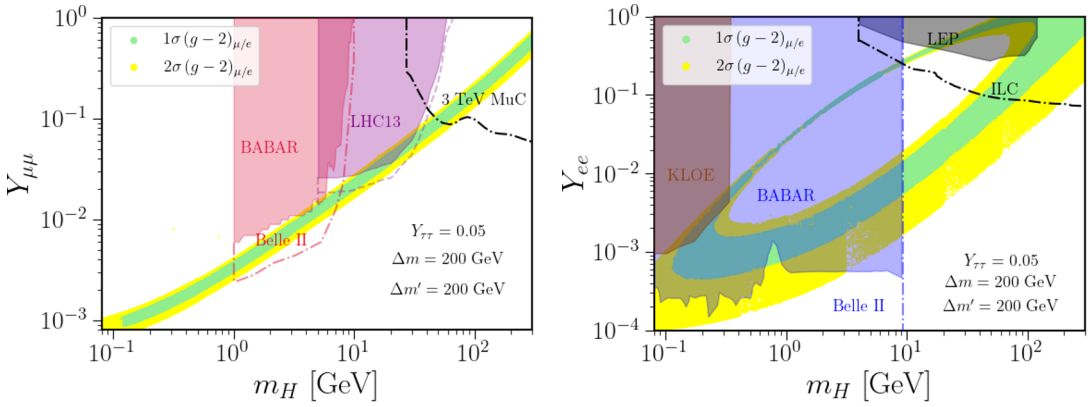

Figure 12. The parameter space of Yukawa couplings ($Y_{\ell\ell}$) vs. scalar boson mass (m_H) satisfying both the AMMs. The green and yellow bands correspond to 1σ and 2σ regions allowed by Δa_ℓ. The shaded regions in the plots indicate the excluded parameter space by different experiments: pink and purple regions are obtained from $e^+e^- \to \mu^+\mu^- H$ searches at BABAR [187] and LHC [188], respectively; blue and brown regions from dark photon searches through $e^+e^- \to \gamma H$ at BABAR [187] and KLOE [215]. Black shaded region is excluded from $e^+e^- \to e^+e^- H$ searches at LEP [221, 224]. Blue and pink dash-dotted are the projected sensitivities from dark-photon searches at Belle-II [231, 232] through $e^+e^- \to \gamma H$ and $e^+e^- \to \mu^+\mu^- H$ searches, respectively. The black dash-dotted line on the left plot shows the projected sensitivity reach on $Y_{\mu\mu}$ from direct searches in the $\mu^+\mu^- \to \mu^+\mu^-\,(H \to \mu^+\mu^-)$ channel at the 3 TeV Muon Collider assuming $\mathcal{L} = 1\,\text{ab}^{-1}$ (cf. figure 11), and the one on the right plot shows the projected upper limits on Y_{ee} from direct searches in the $e^+e^- \to e^+e^-\,(H \to e^+e^-)$ channel at the 1 TeV ILC assuming $\mathcal{L} = 500\,\text{fb}^{-1}$ (cf. figure 8). The pink (purple) shaded region on the left plot assumes the $\text{BR}(H \to \mu\mu) = 1\,(0.5)$ with the purple dotted line $\text{BR}(H \to \mu\mu) = 1$. Here, $\Delta m = m_A - m_H$ and $\Delta m' = m_{H^+} - m_H$.

where $\widehat{M}_\nu$ is the diagonal mass matrix, and U is the 3×3 PMNS lepton mixing matrix. We diagonalize the mass matrix numerically by scanning over the input parameters while being consistent with Δa_ℓ and LFV constraints. For the ease of satisfying the flavor constraints on the Yukawa coupling f, we factor out $f_{\mu\tau}$ into the overall factor and define $a_0 = \kappa f_{\mu\tau}$, where κ is the one-loop factor given in eq. (2.8). Moreover, we perform a constrained minimization where the observables are confined to 3σ of their experimental measured values. The fits to the two textures discussed in eq. (6.1) are shown in the subsequent sections. It is beyond the scope of this work to explore the entire parameter space of the theory; instead, we find benchmark points to show that the model is consistent with neutrino oscillation data while explaining the anomalies for both textures. As was eluded to earlier, we choose the masses of the scalar bosons such that the major contributions to the AMMs appear from the $\mathcal{CP}$-even Higgs H, taking all the other scalars heavier, i.e., fixing $\Delta m (\equiv m_A - m_H) = 200\,\text{GeV}$ and $\Delta m' (\equiv m_{H^+} - m_H) = 200\,\text{GeV}$.

8.1 Fit to `TX-I`

The allowed parameter space of the flavor structure of `TX-I` in eq. (6.1) is explored here, as shown in figure 12. The green and yellow bands in both plots correspond to 1σ and 2σ regions that can simultaneously explain both the AMMs. Here we fix $Y_{\tau\tau} = 0.05$ such that

JHEP03(2022)183

it provides the required sign for Δa_e from the Barr-Zee diagram. Note, a smaller value of the $Y_{\tau\tau}$ requires a larger $Y_{ii}(i \neq \tau)$ to satisfy AMMs, excluding more parameter ranges. On the other hand, making $Y_{\tau\tau}$ larger does allow wider parameter space as the plot in figure 12 would shift downwards. However, it conflicts with the fit to neutrino oscillation data as there would be a large hierarchy in the elements of the neutrino mass matrix. The various shaded regions in figure 12 are excluded from various experimental constraints. The pink and purple shaded regions in figure 12 are excluded from $e^+e^- \to \mu^+\mu^- H$ searches at BaBar [187] and LHC [188]. Here we considered BR($H \to \mu\mu$)=1 (dotted line) and 0.5 (purple shaded region) to show that more parameter space is allowed for $BR < 1$. Blue and brown regions in the right plot are exclusion regions from the dark photon searches through $e^+e^- \to \gamma A_d$ channel at BABAR [187] and KLOE [215]. The combination of these constraints on Yukawa couplings Y_{ee} and $Y_{\mu\mu}$ would exclude light scalar mass below 10 GeV in the parameter space of our interest. The black region is obtained from LEP [221] constraints through $e^+e^- \to e^+e^-(H \to e^+e^-)$ searches, and the black dash-dotted line shows the projected sensitivity at 1 TeV ILC machine (3 TeV Muon Collider), as discussed in section 7.1 (section 7.3). As it can be seen from the figure that though LEP bound does not constrain the parameter space much, ILC would be able to probe a substantial parameter space. For instance, at $m_H = 100$ GeV, the ILC would be sensitive to $Y_{ee} \gtrsim 0.085$ at 2σ. Our results for the fit to the TX-I of eq. (6.1) is shown below:

Fit (TX-I). With $a_0 = \kappa\ f_{\mu\tau} = 2.95 \times 10^{-7}$ and $m_H = 85$ GeV,

$$f = f_{\mu\tau} \begin{pmatrix} 0 & 2.14 \times 10^{-3} & 1.18 \times 10^{-4} \\ 0 & 1 & \\ & 0 & \end{pmatrix}, \quad y = \begin{pmatrix} 0.31 & 0 & 0 \\ 0 & 0.169 & -4.4 \times 10^{-4} \\ 0 & 2.6 \times 10^{-5} & 0.01 \end{pmatrix}. \tag{8.2}$$

For the Yukawa texture above, the corresponding fit for the neutrino oscillation parameters and Δa_ℓ are shown in table 7 as Model `Fit I`. Here the diagonal entries Y_{ii} explain AMMs, while the rest of the Yukawa couplings are required to fit the neutrino oscillation data. It is important to point out that for the texture given in eq. (8.2), $Y_{\mu\mu} \simeq Y_{\tau\tau} m_\tau/m_\mu$ is required to get a NH solution while being consistent with the LFV from $\tau \to \mu\gamma$ and $\tau \to 3\mu$. Thus, for a larger value of $Y_{\tau\tau}$, say 0.05, $Y_{\mu\mu} \simeq 0.8$ is required to get NH solution. For such a large Yukawa coupling, AMM can be satisfied by increasing the scalar mass to about 300 GeV. As noted in section 4, order one coupling Y_{ee} can also induce NSI; for the benchmark point $Y_{ee} = 0.31, \varphi = 0.1$, and $m_{H^+} = 285$ GeV ($\Delta m' = 200$ GeV), we find $\varepsilon_{ee} = 4.2\%$. This can be improved up to 8% [17] with a proper choice of parameters and is limited by direct experimental searches TEXONO [233].

8.2 Fit to `TX-II`

The parameter space explored in `TX-II` of eq. (6.1) is provided in this section. As aforementioned, off-diagonal couplings $Y_{e\mu}$ and $Y_{\mu e}$ need to take opposite signs to get a negative Δa_e from the chirally-enhanced part of eq. (3.2). Furthermore, one of the two couplings needs to be large to provide the required correction to Δa_μ via the non-chiral part of eq. (3.2). The allowed parameter space as a function of Yukawa couplings and scalar mass is shown in

JHEP03(2022)183

Oscillation parameters	$3\,\sigma$ allowed range from NuFit5.1 [234]	Model Fit I	Model Fit II
$\sin^2\theta_{12}$	0.269–0.343	0.314	0.315
$\sin^2\theta_{13}$	0.02032–0.02410	0.02244	0.0219
$\sin^2\theta_{23}$	0.415–0.616	0.527	0.578
Δm^2_{21} $(10^{-5}\ \text{eV}^2)$	6.82–8.04	7.42	7.35
Δm^2_{23} $(10^{-3}\ \text{eV}^2)$	2.435–2.598	2.52	2.52
Observable	**$1\,\sigma$ allowed range**		
Δa_e (10^{-14})	-88 ± 36	-56	-62
Δa_μ (10^{-10})	25 ± 6	29	21

Table 7. Fits to the neutrino oscillation parameters in the model with normal hierarchy, along with Δa_e and Δa_μ for the two benchmark fits given in eq. (8.2) and eq. (8.3). For comparison, the 3σ allowed range for the oscillation parameters and 1σ for Δa_ℓ are also given.

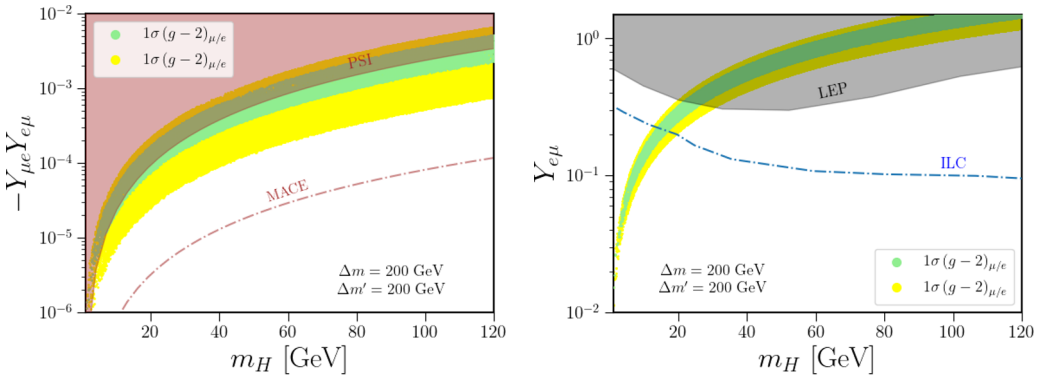

Figure 13. The parameter space of the Yukawa couplings $Y_{e\mu}Y_{\mu e}$ (left) and $Y_{e\mu}$ (right) as a function of scalar mass (m_H) satisfying both AMMs. The green and yellow band in both the figures respectively represents 1σ and 2σ allowed region. The region shaded in gray is excluded by the muonium oscillation PSI experiment [203], whereas the dash-dotted line represents the future sensitivity bound from the MACE experiment [210]. Black shaded region is excluded from $e^+e^- \to e^\pm\mu^\mp H$ searches at LEP [221, 224], whereas blue dash-dotted line is the projected sensitivity from ILC with $\sqrt{s} = 1\,\text{TeV}$ with integrated luminosity $\mathcal{L} = 500\,\text{fb}^-1$.

figure 13, where the green and yellow bands correspond to 1σ and 2σ regions of $\Delta a_{\mu/e}$. The same couplings that give rise to $\Delta a_{e/\mu}$ also induce muonium oscillations, and the probability of these oscillations at the PSI experiment [203] excludes a considerable region of the allowed parameter space, with a lower bound on the scalar mass of 8 (1) GeV at 1σ (2σ). These bounds are expected to improve at the MACE experiment [210] that can probe/exclude all the allowed parameter space. These couplings are directly accessible at lepton colliders via searches in the $e^+e^- \to e^\pm\mu^\mp(H \to e^\pm\mu^\mp)$ channel and can be used to obtain the bound from LEP [221] as shown by the black shaded region in figure 13. The LEP bound imposes an upper limit of about 30 GeV on the scalar mass with the simultaneous explanation of

JHEP03(2022)183

$\Delta a_{e/\mu}$. Furthermore, the projected sensitivity of Yukawa coupling $Y_{e\mu}$ from ILC is shown in the dash-dotted line, which can probe $Y_{e\mu}$ up to ~ 0.1 at $m_H = 100\,\text{GeV}$ and explore the parameter space for AMMs as low as 20 GeV scalar mass. Our results for the fit to the `TX-II` of eq. (6.1) is shown below:

Fit II (`TX-II`). With $a_0 = \kappa\ f_{\mu\tau} = 1.80 \times 10^{-6}$ and $m_H = 22\,\text{GeV}$,

$$f = f_{\mu\tau} \begin{pmatrix} 0 & 0.119 & -0.198 \\ & 0 & 1.0 \\ & & 0 \end{pmatrix}, \qquad y = \begin{pmatrix} 0 & 0.3 & 0 \\ -3.5 \times 10^{-4} & 0 & 5.56 \times 10^{-5} \\ 1.18 \times 10^{-5} & 0 & 5.19 \times 10^{-6} \end{pmatrix}. \tag{8.3}$$

The corresponding fit for the neutrino oscillation and Δa_ℓ are shown in table 7 as Model `Fit II`. The fits are in excellent agreement with the observed experimental values. Here the non-zero Yukawa couplings are introduced to get the neutrino oscillation fit, whereas 0's in the texture are to satisfy LFV such as $\mu \to e\gamma$ and $\tau \to e\mu\mu$. It is worth pointing out that although it is ideal to choose $Y_{e\mu} \sim \mathcal{O}(1)$ instead of $Y_{e\mu}$ such that it can induce diagonal NSI, $\varepsilon_{\mu\mu}$, there is no solution to neutrino oscillation data while simultaneously explaining Δa_ℓ and satisfying flavor constraints.

9 Conclusion

In conclusion, we have proposed a novel scenario in a radiative neutrino mass model, namely the Zee Model, that solves the intriguing deviations observed in muon and electron AMMs simultaneously within 1σ uncertainty, while being consistent with neutrino oscillation data, as well as all the relevant flavor and collider constraints. The neutral scalar in the second Higgs doublet is responsible for explaining both of these anomalies via one-loop and two-loop contributions. The two-loop Barr-Zee diagram is essential for getting the negative correction to a_e. Furthermore, by exhausting all the possibilities, we find two minimum textures in the model that can incorporate both of these anomalies and have a consistent neutrino oscillation fit. We observe that the currently allowed parameter space accommodates the scalar mass in the range of roughly 10–300 GeV in `TX-I` and 1–30 GeV in `TX-II`. In `TX-I`, for $m_H > 200\,\text{GeV}$ ($m_H > 40\,\text{GeV}$), direct searches in the $e^+e^- \to e^+e^-(H \to e^+e^-)$ channel at the 1 TeV ILC would be able to probe all allowed parameter space points with $Y_{ee} \gtrsim 0.07$ ($Y_{ee} > 0.1$) at 2σ uncertainty. Similarly, through searches in the $\mu^+\mu^- \to \mu^+\mu^-(H \to \mu^+\mu^-)$ chanel, the 3 TeV MuC collider would be able to probe the entire region with $m_H \gtrsim 40\,\text{GeV}$ irrespective of $Y_{\mu\mu}$. In `TX-II`, we observe that all allowed parameter space points with $m_H > 20\,\text{GeV}$ fall within the projected exclusion reach of 1 TeV ILC via searches in the $e^+e^- \to \mu^+e^-(H \to \mu^+e^-)$ channel. The model also features charged scalars required for generating neutrino masses which induce diagonal NSI ε_{ee} as large as 8%. Furthermore, the model can also give a sizable EDM of muon that can potentially be measured in future experiments. This task of connecting both the AMMs and finding textures to get neutrino oscillation fit is a highly non-trivial. As we have shown in detail, the allowed parameter space in the model can be probed in future experiments, which will either discover NP or rule out the possibility of explaining both AMMs within the context of the Zee Model.

JHEP03(2022)183

Acknowledgments

We would like to thank K.S. Babu, Ahmed Ismail and Julian Heeck for useful discussion. RKB and RD thank the U.S. Department of Energy for the financial support, under grant number DE-SC 0016013. Some computing for this project was performed at the High Performance Computing Center at Oklahoma State University, supported in part through the National Science Foundation grant OAC-1531128.

A AMM expressions

A.1 One-loop

In the limit $m_i \ll m_\phi$ the expression for one-loop contribution to AMM [235] from neutral scalars simplifies to

$$\Delta a_\ell^{(1)}(\phi) = \frac{1}{16\pi^2}\frac{m_\ell^2}{m_\phi^2}\left(\frac{|Y_{\ell i}|^2+|Y_{i\ell}|^2}{6} \mp 2\frac{m_i}{m_\ell}\left(\frac{3}{4}+\log\left(\frac{m_i}{m_\phi}\right)\right)\mathrm{Re}(Y_{\ell i}Y_{i\ell})\right). \tag{A.1}$$

In the expression above, $-$ and $+$ correspond to H and A, respectively. Similarly, the charged scalar contribution is simply

$$\Delta a_\ell^{(1)}(H^+) = \frac{-1}{96\pi^2}\frac{m_\ell^2}{m_{H^+}^2}|Y_{i\ell}|^2. \tag{A.2}$$

A.2 Two-loop

The loop functions are

$$G(z,1) = \begin{cases} 2\left[(2+\log z)+\dfrac{1-2z}{\sqrt{1-4z}}\left\{Li_2\left(\dfrac{x_-}{x_+}\right)-Li_2\left(\dfrac{x_+}{x_-}\right)\right\}\right] & \text{for } z<\dfrac{1}{4}, \\ 4 & \text{for } z=\dfrac{1}{4}, \\ 2(2+\log z)-\dfrac{2i(2z-1)}{\sqrt{4z-1}}\left[\log z\log\dfrac{y_-}{y_+}-Li_2\left(\dfrac{2i}{y_+}\right)+Li_2\left(\dfrac{-2i}{y_-}\right)\right] & \text{for } z>\dfrac{1}{4} \end{cases} \tag{A.3}$$

$$G(z,0) = \begin{cases} \dfrac{2}{\sqrt{1-4z}}\left[Li_2\left(\dfrac{x_-}{x_+}\right)-Li_2\left(\dfrac{x_+}{x_-}\right)\right] & \text{for } z<\dfrac{1}{4}, \\ 2\ \log 16 & \text{for } z=\dfrac{1}{4}, \\ \dfrac{2i}{\sqrt{4z-1}}\left[\log z\log\left(\dfrac{y_-}{y_+}\right)+Li_2\left(\dfrac{-2i}{y_-}\right)-Li_2\left(\dfrac{2i}{y_+}\right)\right] & \text{for } z>\dfrac{1}{4}, \end{cases} \tag{A.4}$$

where, $x_\pm = \sqrt{1-4z}\pm 1$, $y_\pm = \sqrt{4z-1}\pm i$ and $z = m_i^2/m_\phi^2$.

JHEP03(2022)183

References

[1] Particle Data Group collaboration, *Review of Particle Physics*, *PTEP* **2020** (2020) 083C01 [INSPIRE].

[2] S. Weinberg, *Baryon and Lepton Nonconserving Processes*, *Phys. Rev. Lett.* **43** (1979) 1566 [INSPIRE].

[3] P. Minkowski, $\mu \to e\gamma$ *at a Rate of One Out of* 10^9 *Muon Decays?*, *Phys. Lett. B* **67** (1977) 421 [INSPIRE].

[4] R.N. Mohapatra and G. Senjanović, *Neutrino Mass and Spontaneous Parity Nonconservation*, *Phys. Rev. Lett.* **44** (1980) 912 [INSPIRE].

[5] T. Yanagida, *Horizontal Symmetry and Masses of Neutrinos*, *Prog. Theor. Phys.* **64** (1980) 1103 [INSPIRE].

[6] M. Gell-Mann, P. Ramond and R. Slansky, *Complex Spinors and Unified Theories*, *Conf. Proc. C* **790927** (1979) 315 [arXiv:1306.4669] [INSPIRE].

[7] S.L. Glashow, *The Future of Elementary Particle Physics*, *NATO Sci. Ser. B* **61** (1980) 687 [INSPIRE].

[8] J. Schechter and J.W.F. Valle, *Neutrino Masses in* SU(2) × U(1) *Theories*, *Phys. Rev. D* **22** (1980) 2227 [INSPIRE].

[9] T.P. Cheng and L.-F. Li, *Neutrino Masses, Mixings and Oscillations in* SU(2) × U(1) *Models of Electroweak Interactions*, *Phys. Rev. D* **22** (1980) 2860 [INSPIRE].

[10] R.N. Mohapatra and G. Senjanović, *Neutrino Masses and Mixings in Gauge Models with Spontaneous Parity Violation*, *Phys. Rev. D* **23** (1981) 165 [INSPIRE].

[11] G. Lazarides, Q. Shafi and C. Wetterich, *Proton Lifetime and Fermion Masses in an* SO(10) *Model*, *Nucl. Phys. B* **181** (1981) 287 [INSPIRE].

[12] R. Foot, H. Lew, X.G. He and G.C. Joshi, *Seesaw Neutrino Masses Induced by a Triplet of Leptons*, *Z. Phys. C* **44** (1989) 441 [INSPIRE].

[13] A. Zee, *A Theory of Lepton Number Violation, Neutrino Majorana Mass, and Oscillation*, *Phys. Lett. B* **93** (1980) 389 [*Erratum ibid.* **95** (1980) 461] [INSPIRE].

[14] A. Zee, *Quantum Numbers of Majorana Neutrino Masses*, *Nucl. Phys. B* **264** (1986) 99 [INSPIRE].

[15] K.S. Babu, E. Ma and J.T. Pantaleone, *Model of Radiative Neutrino Masses: Mixing and a Possible Fourth Generation*, *Phys. Lett. B* **218** (1989) 233 [INSPIRE].

[16] Y. Cai, J. Herrero-García, M.A. Schmidt, A. Vicente and R.R. Volkas, *From the trees to the forest: a review of radiative neutrino mass models*, *Front. in Phys.* **5** (2017) 63 [arXiv:1706.08524] [INSPIRE].

[17] K.S. Babu, P.S.B. Dev, S. Jana and A. Thapa, *Non-Standard Interactions in Radiative Neutrino Mass Models*, *JHEP* **03** (2020) 006 [arXiv:1907.09498] [INSPIRE].

[18] J.S. Schwinger, *On Quantum electrodynamics and the magnetic moment of the electron*, *Phys. Rev.* **73** (1948) 416 [INSPIRE].

[19] P. Kusch and H.M. Foley, *The Magnetic Moment of the Electron*, *Phys. Rev.* **74** (1948) 250 [INSPIRE].

[20] C.M. Sommerfield, *Magnetic Dipole Moment of the Electron*, *Phys. Rev.* **107** (1957) 328 [INSPIRE].

JHEP03(2022)183

[21] A. Petermann, *Fourth order magnetic moment of the electron*, *Helv. Phys. Acta* **30** (1957) 407 [INSPIRE].

[22] T. Kinoshita and W.B. Lindquist, *Eighth Order Anomalous Magnetic Moment of the electron*, *Phys. Rev. Lett.* **47** (1981) 1573 [INSPIRE].

[23] T. Kinoshita, B. Nizic and Y. Okamoto, *Eighth order QED contribution to the anomalous magnetic moment of the muon*, *Phys. Rev. D* **41** (1990) 593 [INSPIRE].

[24] S. Laporta and E. Remiddi, *The Analytical value of the electron $(g-2)$ at order α^3 in QED*, *Phys. Lett. B* **379** (1996) 283 [hep-ph/9602417] [INSPIRE].

[25] G. Degrassi and G.F. Giudice, *QED logarithms in the electroweak corrections to the muon anomalous magnetic moment*, *Phys. Rev. D* **58** (1998) 053007 [hep-ph/9803384] [INSPIRE].

[26] A. Czarnecki and W.J. Marciano, *Lepton anomalous magnetic moments: A Theory update*, *Nucl. Phys. B Proc. Suppl.* **76** (1999) 245 [hep-ph/9810512] [INSPIRE].

[27] T. Kinoshita and M. Nio, *Improved α^4 term of the muon anomalous magnetic moment*, *Phys. Rev. D* **70** (2004) 113001 [hep-ph/0402206] [INSPIRE].

[28] T. Kinoshita and M. Nio, *The Tenth-order QED contribution to the lepton $g-2$: Evaluation of dominant α^5 terms of muon $g-2$*, *Phys. Rev. D* **73** (2006) 053007 [hep-ph/0512330] [INSPIRE].

[29] M. Passera, *Precise mass-dependent QED contributions to leptonic $g-2$ at order α^2 and α^3*, *Phys. Rev. D* **75** (2007) 013002 [hep-ph/0606174] [INSPIRE].

[30] A.L. Kataev, *Reconsidered estimates of the 10th order QED contributions to the muon anomaly*, *Phys. Rev. D* **74** (2006) 073011 [hep-ph/0608120] [INSPIRE].

[31] T. Aoyama, M. Hayakawa, T. Kinoshita and M. Nio, *Revised value of the eighth-order QED contribution to the anomalous magnetic moment of the electron*, *Phys. Rev. D* **77** (2008) 053012 [arXiv:0712.2607] [INSPIRE].

[32] S.G. Karshenboim, *New recommended values of the fundamental physical constants (CODATA 2006)*, *Phys. Usp.* **51** (2008) 1019.

[33] T. Aoyama, M. Hayakawa, T. Kinoshita and M. Nio, *Complete Tenth-Order QED Contribution to the Muon $g-2$*, *Phys. Rev. Lett.* **109** (2012) 111808 [arXiv:1205.5370] [INSPIRE].

[34] O. Schnetz, *The Galois coaction on the electron anomalous magnetic moment*, *Commun. Num. Theor. Phys.* **12** (2018) 335 [arXiv:1711.05118] [INSPIRE].

[35] T. Aoyama, T. Kinoshita and M. Nio, *Revised and Improved Value of the QED Tenth-Order Electron Anomalous Magnetic Moment*, *Phys. Rev. D* **97** (2018) 036001 [arXiv:1712.06060] [INSPIRE].

[36] S. Volkov, *New method of computing the contributions of graphs without lepton loops to the electron anomalous magnetic moment in QED*, *Phys. Rev. D* **96** (2017) 096018 [arXiv:1705.05800] [INSPIRE].

[37] S. Volkov, *Numerical calculation of high-order QED contributions to the electron anomalous magnetic moment*, *Phys. Rev. D* **98** (2018) 076018 [arXiv:1807.05281] [INSPIRE].

[38] A. Czarnecki, B. Krause and W.J. Marciano, *Electroweak Fermion loop contributions to the muon anomalous magnetic moment*, *Phys. Rev. D* **52** (1995) R2619 [hep-ph/9506256] [INSPIRE].

JHEP03(2022)183

[39] A. Czarnecki, B. Krause and W.J. Marciano, *Electroweak corrections to the muon anomalous magnetic moment*, *Phys. Rev. Lett.* **76** (1996) 3267 [hep-ph/9512369] [INSPIRE].

[40] A. Czarnecki and B. Krause, *Electroweak corrections to the muon anomalous magnetic moment*, *Nucl. Phys. B Proc. Suppl.* **51** (1996) 148 [hep-ph/9606393] [INSPIRE].

[41] A. Czarnecki, W.J. Marciano and A. Vainshtein, *Refinements in electroweak contributions to the muon anomalous magnetic moment*, *Phys. Rev. D* **67** (2003) 073006 [*Erratum ibid.* **73** (2006) 119901] [hep-ph/0212229] [INSPIRE].

[42] S. Heinemeyer, D. Stöckinger and G. Weiglein, *Electroweak and supersymmetric two-loop corrections to* $(g-2)_\mu$, *Nucl. Phys. B* **699** (2004) 103 [hep-ph/0405255] [INSPIRE].

[43] T. Gribouk and A. Czarnecki, *Electroweak interactions and the muon* $g-2$*: Bosonic two-loop effects*, *Phys. Rev. D* **72** (2005) 053016 [hep-ph/0509205] [INSPIRE].

[44] C. Gnendiger, D. Stöckinger and H. Stöckinger-Kim, *The electroweak contributions to* $(g-2)_\mu$ *after the Higgs boson mass measurement*, *Phys. Rev. D* **88** (2013) 053005 [arXiv:1306.5546] [INSPIRE].

[45] F. Jegerlehner, *Hadronic Contributions to Electroweak Parameter Shifts: A Detailed Analysis*, *Z. Phys. C* **32** (1986) 195 [INSPIRE].

[46] B.W. Lynn, G. Penso and C. Verzegnassi, *Strong interaction contributions to one loop leptonic process*, *Phys. Rev. D* **35** (1987) 42 [INSPIRE].

[47] M.L. Swartz, *Reevaluation of the hadronic contribution to* $\alpha(M_Z^2)$, *Phys. Rev. D* **53** (1996) 5268 [hep-ph/9509248] [INSPIRE].

[48] A.D. Martin and D. Zeppenfeld, *A Determination of the QED coupling at the Z pole*, *Phys. Lett. B* **345** (1995) 558 [hep-ph/9411377] [INSPIRE].

[49] S. Eidelman, F. Jegerlehner, A.L. Kataev and O. Veretin, *Testing nonperturbative strong interaction effects via the Adler function*, *Phys. Lett. B* **454** (1999) 369 [hep-ph/9812521] [INSPIRE].

[50] B. Krause, *Higher order hadronic contributions to the anomalous magnetic moment of leptons*, *Phys. Lett. B* **390** (1997) 392 [hep-ph/9607259] [INSPIRE].

[51] M. Davier and A. Hocker, *New results on the hadronic contributions to* $\alpha(M_Z^2)$ *and to* $(g-2)_\mu$, *Phys. Lett. B* **435** (1998) 427 [hep-ph/9805470] [INSPIRE].

[52] F. Jegerlehner, *Theoretical precision in estimates of the hadronic contributions to* $(g-2)_\mu$ *and* $\alpha_{QED}(M_Z)$, *Nucl. Phys. B Proc. Suppl.* **126** (2004) 325 [hep-ph/0310234] [INSPIRE].

[53] J.F. de Troconiz and F.J. Yndurain, *The Hadronic contributions to the anomalous magnetic moment of the muon*, *Phys. Rev. D* **71** (2005) 073008 [hep-ph/0402285] [INSPIRE].

[54] M. Davier, *The Hadronic contribution to* $(g-2)_\mu$, *Nucl. Phys. B Proc. Suppl.* **169** (2007) 288 [hep-ph/0701163] [INSPIRE].

[55] F. Campanario et al., *Standard model radiative corrections in the pion form factor measurements do not explain the* a_μ *anomaly*, *Phys. Rev. D* **100** (2019) 076004 [arXiv:1903.10197] [INSPIRE].

[56] M. Davier, A. Hoecker, B. Malaescu and Z. Zhang, *Reevaluation of the hadronic vacuum polarisation contributions to the Standard Model predictions of the muon* $g-2$ *and* $\alpha(m_Z^2)$ *using newest hadronic cross-section data*, *Eur. Phys. J. C* **77** (2017) 827 [arXiv:1706.09436] [INSPIRE].

JHEP03(2022)183

[57] A. Keshavarzi, D. Nomura and T. Teubner, *Muon $g-2$ and $\alpha(M_Z^2)$: a new data-based analysis*, *Phys. Rev. D* **97** (2018) 114025 [arXiv:1802.02995] [INSPIRE].

[58] G. Colangelo, M. Hoferichter and P. Stoffer, *Two-pion contribution to hadronic vacuum polarization*, *JHEP* **02** (2019) 006 [arXiv:1810.00007] [INSPIRE].

[59] M. Hoferichter, B.-L. Hoid and B. Kubis, *Three-pion contribution to hadronic vacuum polarization*, *JHEP* **08** (2019) 137 [arXiv:1907.01556] [INSPIRE].

[60] M. Davier, A. Hoecker, B. Malaescu and Z. Zhang, *A new evaluation of the hadronic vacuum polarisation contributions to the muon anomalous magnetic moment and to $\alpha(m_Z^2)$*, *Eur. Phys. J. C* **80** (2020) 241 [*Erratum ibid.* **80** (2020) 410] [arXiv:1908.00921] [INSPIRE].

[61] A. Keshavarzi, D. Nomura and T. Teubner, *$g-2$ of charged leptons, $\alpha(M_Z^2)$, and the hyperfine splitting of muonium*, *Phys. Rev. D* **101** (2020) 014029 [arXiv:1911.00367] [INSPIRE].

[62] A. Kurz, T. Liu, P. Marquard and M. Steinhauser, *Hadronic contribution to the muon anomalous magnetic moment to next-to-next-to-leading order*, *Phys. Lett. B* **734** (2014) 144 [arXiv:1403.6400] [INSPIRE].

[63] J. Bijnens, E. Pallante and J. Prades, *Analysis of the hadronic light by light contributions to the muon $g-2$*, *Nucl. Phys. B* **474** (1996) 379 [hep-ph/9511388] [INSPIRE].

[64] M. Hayakawa and T. Kinoshita, *Pseudoscalar pole terms in the hadronic light by light scattering contribution to muon $g-2$*, *Phys. Rev. D* **57** (1998) 465 [*Erratum ibid.* **66** (2002) 019902] [hep-ph/9708227] [INSPIRE].

[65] M. Knecht and A. Nyffeler, *Hadronic light by light corrections to the muon $g-2$: The Pion pole contribution*, *Phys. Rev. D* **65** (2002) 073034 [hep-ph/0111058] [INSPIRE].

[66] M. Knecht, A. Nyffeler, M. Perrottet and E. de Rafael, *Hadronic light by light scattering contribution to the muon $g-2$: An Effective field theory approach*, *Phys. Rev. Lett.* **88** (2002) 071802 [hep-ph/0111059] [INSPIRE].

[67] M.J. Ramsey-Musolf and M.B. Wise, *Hadronic light by light contribution to muon $g-2$ in chiral perturbation theory*, *Phys. Rev. Lett.* **89** (2002) 041601 [hep-ph/0201297] [INSPIRE].

[68] K. Melnikov and A. Vainshtein, *Hadronic light-by-light scattering contribution to the muon anomalous magnetic moment revisited*, *Phys. Rev. D* **70** (2004) 113006 [hep-ph/0312226] [INSPIRE].

[69] J. Bijnens and J. Prades, *The Hadronic Light-by-Light Contribution to the Muon Anomalous Magnetic Moment: Where do we stand?*, *Mod. Phys. Lett. A* **22** (2007) 767 [hep-ph/0702170] [INSPIRE].

[70] J. Prades, E. de Rafael and A. Vainshtein, *The Hadronic Light-by-Light Scattering Contribution to the Muon and Electron Anomalous Magnetic Moments*, *Adv. Ser. Direct. High Energy Phys.* **20** (2009) 303 [arXiv:0901.0306] [INSPIRE].

[71] A.L. Kataev, *Analytical eighth-order light-by-light QED contributions from leptons with heavier masses to the anomalous magnetic moment of electron*, *Phys. Rev. D* **86** (2012) 013010 [arXiv:1205.6191] [INSPIRE].

[72] P. Masjuan and P. Sanchez-Puertas, *Pseudoscalar-pole contribution to the $(g_\mu-2)$: a rational approach*, *Phys. Rev. D* **95** (2017) 054026 [arXiv:1701.05829] [INSPIRE].

[73] G. Colangelo, M. Hoferichter, M. Procura and P. Stoffer, *Dispersion relation for hadronic light-by-light scattering: two-pion contributions*, *JHEP* **04** (2017) 161 [arXiv:1702.07347] [INSPIRE].

JHEP03(2022)183

[74] M. Hoferichter, B.-L. Hoid, B. Kubis, S. Leupold and S.P. Schneider, *Dispersion relation for hadronic light-by-light scattering: pion pole*, *JHEP* **10** (2018) 141 [arXiv:1808.04823] [INSPIRE].

[75] A. Gérardin, H.B. Meyer and A. Nyffeler, *Lattice calculation of the pion transition form factor with $N_f = 2 + 1$ Wilson quarks*, *Phys. Rev. D* **100** (2019) 034520 [arXiv:1903.09471] [INSPIRE].

[76] J. Bijnens, N. Hermansson-Truedsson and A. Rodríguez-Sánchez, *Short-distance constraints for the HLbL contribution to the muon anomalous magnetic moment*, *Phys. Lett. B* **798** (2019) 134994 [arXiv:1908.03331] [INSPIRE].

[77] G. Colangelo, F. Hagelstein, M. Hoferichter, L. Laub and P. Stoffer, *Longitudinal short-distance constraints for the hadronic light-by-light contribution to $(g-2)_\mu$ with large-N_c Regge models*, *JHEP* **03** (2020) 101 [arXiv:1910.13432] [INSPIRE].

[78] G. Colangelo, M. Hoferichter, A. Nyffeler, M. Passera and P. Stoffer, *Remarks on higher-order hadronic corrections to the muon g−2*, *Phys. Lett. B* **735** (2014) 90 [arXiv:1403.7512] [INSPIRE].

[79] V. Pauk and M. Vanderhaeghen, *Single meson contributions to the muon's anomalous magnetic moment*, *Eur. Phys. J. C* **74** (2014) 3008 [arXiv:1401.0832] [INSPIRE].

[80] I. Danilkin and M. Vanderhaeghen, *Light-by-light scattering sum rules in light of new data*, *Phys. Rev. D* **95** (2017) 014019 [arXiv:1611.04646] [INSPIRE].

[81] F. Jegerlehner, *The Anomalous Magnetic Moment of the Muon*, vol. 274, Springer, Cham (2017) [DOI] [INSPIRE].

[82] M. Knecht, S. Narison, A. Rabemananjara and D. Rabetiarivony, *Scalar meson contributions to a μ from hadronic light-by-light scattering*, *Phys. Lett. B* **787** (2018) 111 [arXiv:1808.03848] [INSPIRE].

[83] G. Eichmann, C.S. Fischer and R. Williams, *Kaon-box contribution to the anomalous magnetic moment of the muon*, *Phys. Rev. D* **101** (2020) 054015 [arXiv:1910.06795] [INSPIRE].

[84] P. Roig and P. Sanchez-Puertas, *Axial-vector exchange contribution to the hadronic light-by-light piece of the muon anomalous magnetic moment*, *Phys. Rev. D* **101** (2020) 074019 [arXiv:1910.02881] [INSPIRE].

[85] T. Blum et al., *Hadronic Light-by-Light Scattering Contribution to the Muon Anomalous Magnetic Moment from Lattice QCD*, *Phys. Rev. Lett.* **124** (2020) 132002 [arXiv:1911.08123] [INSPIRE].

[86] Muon $g-2$ collaboration, *Measurement of the Positive Muon Anomalous Magnetic Moment to 0.46 ppm*, *Phys. Rev. Lett.* **126** (2021) 141801 [arXiv:2104.03281] [INSPIRE].

[87] Muon $g-2$ collaboration, *Final Report of the Muon E821 Anomalous Magnetic Moment Measurement at BNL*, *Phys. Rev. D* **73** (2006) 072003 [hep-ex/0602035] [INSPIRE].

[88] Muon $g-2$ collaboration, *Precise measurement of the positive muon anomalous magnetic moment*, *Phys. Rev. Lett.* **86** (2001) 2227 [hep-ex/0102017] [INSPIRE].

[89] T. Aoyama et al., *The anomalous magnetic moment of the muon in the Standard Model*, *Phys. Rept.* **887** (2020) 1 [arXiv:2006.04822] [INSPIRE].

[90] M. Davier, A. Hoecker, B. Malaescu and Z. Zhang, *Reevaluation of the Hadronic Contributions to the Muon g-2 and to alpha(MZ)*, *Eur. Phys. J. C* **71** (2011) 1515 [*Erratum ibid.* **72** (2012) 1874] [arXiv:1010.4180] [INSPIRE].

JHEP03(2022)183

[91] A. Gérardin, *The anomalous magnetic moment of the muon: status of Lattice QCD calculations*, *Eur. Phys. J. A* **57** (2021) 116 [arXiv:2012.03931] [INSPIRE].

[92] D. Hanneke, S. Fogwell and G. Gabrielse, *New Measurement of the Electron Magnetic Moment and the Fine Structure Constant*, *Phys. Rev. Lett.* **100** (2008) 120801 [arXiv:0801.1134] [INSPIRE].

[93] R.H. Parker, C. Yu, W. Zhong, B. Estey and H. Müller, *Measurement of the fine-structure constant as a test of the Standard Model*, *Science* **360** (2018) 191 [arXiv:1812.04130] [INSPIRE].

[94] T. Aoyama, M. Hayakawa, T. Kinoshita and M. Nio, *Tenth-Order QED Contribution to the Electron g-2 and an Improved Value of the Fine Structure Constant*, *Phys. Rev. Lett.* **109** (2012) 111807 [arXiv:1205.5368] [INSPIRE].

[95] S. Laporta, *High-precision calculation of the 4-loop contribution to the electron $g-2$ in QED*, *Phys. Lett. B* **772** (2017) 232 [arXiv:1704.06996] [INSPIRE].

[96] S. Volkov, *Calculating the five-loop QED contribution to the electron anomalous magnetic moment: Graphs without lepton loops*, *Phys. Rev. D* **100** (2019) 096004 [arXiv:1909.08015] [INSPIRE].

[97] L. Morel, Z. Yao, P. Cladé and S. Guellati-Khélifa, *Determination of the fine-structure constant with an accuracy of 81 parts per trillion*, *Nature* **588** (2020) 61 [INSPIRE].

[98] A. Crivellin, M. Hoferichter and P. Schmidt-Wellenburg, *Combined explanations of $(g-2)_{\mu,e}$ and implications for a large muon EDM*, *Phys. Rev. D* **98** (2018) 113002 [arXiv:1807.11484] [INSPIRE].

[99] G. Hiller, C. Hormigos-Feliu, D.F. Litim and T. Steudtner, *Anomalous magnetic moments from asymptotic safety*, *Phys. Rev. D* **102** (2020) 071901 [arXiv:1910.14062] [INSPIRE].

[100] E.J. Chun and T. Mondal, *Explaining $g-2$ anomalies in two Higgs doublet model with vector-like leptons*, *JHEP* **11** (2020) 077 [arXiv:2009.08314] [INSPIRE].

[101] K.-F. Chen, C.-W. Chiang and K. Yagyu, *An explanation for the muon and electron $g-2$ anomalies and dark matter*, *JHEP* **09** (2020) 119 [arXiv:2006.07929] [INSPIRE].

[102] C. Hati, J. Kriewald, J. Orloff and A.M. Teixeira, *Anomalies in ^{8}Be nuclear transitions and $(g-2)_{e,\mu}$: towards a minimal combined explanation*, *JHEP* **07** (2020) 235 [arXiv:2005.00028] [INSPIRE].

[103] P. Escribano, J. Terol-Calvo and A. Vicente, *$(g-2)_{e,\mu}$ in an extended inverse type-III seesaw model*, *Phys. Rev. D* **103** (2021) 115018 [arXiv:2104.03705] [INSPIRE].

[104] A.E.C. Hernández, S.F. King and H. Lee, *Fermion mass hierarchies from vectorlike families with an extended 2HDM and a possible explanation for the electron and muon anomalous magnetic moments*, *Phys. Rev. D* **103** (2021) 115024 [arXiv:2101.05819] [INSPIRE].

[105] D. Borah, M. Dutta, S. Mahapatra and N. Sahu, *Lepton anomalous magnetic moment with singlet-doublet fermion dark matter in a scotogenic* U(1)$L_\mu - L_\tau$ *model*, *Phys. Rev. D* **105** (2022) 015029 [arXiv:2109.02699] [INSPIRE].

[106] H. Bharadwaj, S. Dutta and A. Goyal, *Leptonic $g-2$ anomaly in an extended Higgs sector with vector-like leptons*, *JHEP* **11** (2021) 056 [arXiv:2109.02586] [INSPIRE].

[107] H. Davoudiasl and W.J. Marciano, *Tale of two anomalies*, *Phys. Rev. D* **98** (2018) 075011 [arXiv:1806.10252] [INSPIRE].

JHEP03(2022)183

[108] J. Liu, C.E.M. Wagner and X.-P. Wang, *A light complex scalar for the electron and muon anomalous magnetic moments*, *JHEP* **03** (2019) 008 [arXiv:1810.11028] [INSPIRE].

[109] X.-F. Han, T. Li, L. Wang and Y. Zhang, *Simple interpretations of lepton anomalies in the lepton-specific inert two-Higgs-doublet model*, *Phys. Rev. D* **99** (2019) 095034 [arXiv:1812.02449] [INSPIRE].

[110] M. Bauer, M. Neubert, S. Renner, M. Schnubel and A. Thamm, *Axionlike Particles, Lepton-Flavor Violation, and a New Explanation of a_μ and a_e*, *Phys. Rev. Lett.* **124** (2020) 211803 [arXiv:1908.00008] [INSPIRE].

[111] C. Cornella, P. Paradisi and O. Sumensari, *Hunting for ALPs with Lepton Flavor Violation*, *JHEP* **01** (2020) 158 [arXiv:1911.06279] [INSPIRE].

[112] B. Dutta, S. Ghosh and T. Li, *Explaining $(g-2)_{\mu,e}$, the KOTO anomaly and the MiniBooNE excess in an extended Higgs model with sterile neutrinos*, *Phys. Rev. D* **102** (2020) 055017 [arXiv:2006.01319] [INSPIRE].

[113] M. Endo, S. Iguro and T. Kitahara, *Probing $e\mu$ flavor-violating ALP at Belle II*, *JHEP* **06** (2020) 040 [arXiv:2002.05948] [INSPIRE].

[114] N. Haba, Y. Shimizu and T. Yamada, *Muon and electron $g-2$ and the origin of the fermion mass hierarchy*, *PTEP* **2020** (2020) 093B05 [arXiv:2002.10230] [INSPIRE].

[115] A.E.C. Hernández, D.T. Huong and I. Schmidt, *Universal inverse seesaw mechanism as a source of the SM fermion mass hierarchy*, *Eur. Phys. J. C* **82** (2022) 63 [arXiv:2109.12118] [INSPIRE].

[116] T. Mondal and H. Okada, *Inverse seesaw and $(g-2)$ anomalies in $B-L$ extended two Higgs doublet model*, *Nucl. Phys. B* **976** (2022) 115716 [arXiv:2103.13149] [INSPIRE].

[117] R. Adhikari, I.A. Bhat, D. Borah, E. Ma and D. Nanda, *Anomalous magnetic moment and Higgs coupling of the muon in a sequential* U(1) *gauge model with dark matter*, *Phys. Rev. D* **105** (2022) 035006 [arXiv:2109.05417] [INSPIRE].

[118] M. Bauer, M. Neubert, S. Renner, M. Schnubel and A. Thamm, *Flavor probes of axion-like particles*, arXiv:2110.10698 [INSPIRE].

[119] B. De, D. Das, M. Mitra and N. Sahoo, *Magnetic Moments of Leptons, Charged Lepton Flavor Violations and Dark Matter Phenomenology of a Minimal Radiative Dirac Neutrino Mass Model*, arXiv:2106.00979 [INSPIRE].

[120] L.T. Hue, A.E.C. Hernández, H.N. Long and T.T. Hong, *Heavy singly charged Higgs bosons and inverse seesaw neutrinos as origins of large $(g-2)_{e,\mu}$ in two Higgs doublet models*, arXiv:2110.01356 [INSPIRE].

[121] W.-Y. Keung, D. Marfatia and P.-Y. Tseng, *Axion-Like Particles, Two-Higgs-Doublet Models, Leptoquarks, and the Electron and Muon $(g-2)$*, *LHEP* **2021** (2021) 209 [arXiv:2104.03341] [INSPIRE].

[122] I. Bigaran and R.R. Volkas, *Getting chirality right: Single scalar leptoquark solutions to the $(g-2)_{e,\mu}$ puzzle*, *Phys. Rev. D* **102** (2020) 075037 [arXiv:2002.12544] [INSPIRE].

[123] I. Doršner, S. Fajfer and S. Saad, *$\mu \to e\gamma$ selecting scalar leptoquark solutions for the $(g-2)_{e,\mu}$ puzzles*, *Phys. Rev. D* **102** (2020) 075007 [arXiv:2006.11624] [INSPIRE].

[124] I. Bigaran and R.R. Volkas, *Reflecting on chirality: CP-violating extensions of the single scalar-leptoquark solutions for the $(g-2)_{e,\mu}$ puzzles and their implications for lepton EDMs*, *Phys. Rev. D* **105** (2022) 015002 [arXiv:2110.03707] [INSPIRE].

JHEP03(2022)183

[125] M. Abdullah, B. Dutta, S. Ghosh and T. Li, $(g-2)_{\mu,e}$ *and the ANITA anomalous events in a three-loop neutrino mass model*, *Phys. Rev. D* **100** (2019) 115006 [arXiv:1907.08109] [INSPIRE].

[126] A.E. Cárcamo Hernández, Y. Hidalgo Velásquez, S. Kovalenko, H.N. Long, N.A. Pérez-Julve and V.V. Vien, *Fermion spectrum and* $g-2$ *anomalies in a low scale 3-3-1 model*, *Eur. Phys. J. C* **81** (2021) 191 [arXiv:2002.07347] [INSPIRE].

[127] A.E. Cárcamo Hernández, S.F. King, H. Lee and S.J. Rowley, *Is it possible to explain the muon and electron* $g-2$ *in a* Z' *model?*, *Phys. Rev. D* **101** (2020) 115016 [arXiv:1910.10734] [INSPIRE].

[128] A. Bodas, R. Coy and S.J.D. King, *Solving the electron and muon* $g-2$ *anomalies in* Z' *models*, *Eur. Phys. J. C* **81** (2021) 1065 [arXiv:2102.07781] [INSPIRE].

[129] T.A. Chowdhury and S. Saad, *Non-Abelian vector dark matter and lepton* $g-2$, *JCAP* **10** (2021) 014 [arXiv:2107.11863] [INSPIRE].

[130] A.E.C. Hernández, S. Kovalenko, M. Maniatis and I. Schmidt, *Fermion mass hierarchy and* $g-2$ *anomalies in an extended 3HDM Model*, *JHEP* **10** (2021) 036 [arXiv:2104.07047] [INSPIRE].

[131] F. He and P. Wang, *Pauli form factors of electron and muon in nonlocal quantum electrodynamics*, *Eur. Phys. J. Plus* **135** (2020) 156 [arXiv:1901.00271] [INSPIRE].

[132] M. Badziak and K. Sakurai, *Explanation of electron and muon* $g-2$ *anomalies in the MSSM*, *JHEP* **10** (2019) 024 [arXiv:1908.03607] [INSPIRE].

[133] M. Endo and W. Yin, *Explaining electron and muon* $g-2$ *anomaly in SUSY without lepton-flavor mixings*, *JHEP* **08** (2019) 122 [arXiv:1906.08768] [INSPIRE].

[134] X.-X. Dong, S.-M. Zhao, H.-B. Zhang and T.-F. Feng, *The two-loop corrections to lepton MDMs and EDMs in the EBLMSSM*, *J. Phys. G* **47** (2020) 045002 [arXiv:1901.07701] [INSPIRE].

[135] J.-L. Yang, T.-F. Feng and H.-B. Zhang, *Electron and muon* $(g-2)$ *in the B-LSSM*, *J. Phys. G* **47** (2020) 055004 [arXiv:2003.09781] [INSPIRE].

[136] J. Cao, Y. He, J. Lian, D. Zhang and P. Zhu, *Electron and muon anomalous magnetic moments in the inverse seesaw extended NMSSM*, *Phys. Rev. D* **104** (2021) 055009 [arXiv:2102.11355] [INSPIRE].

[137] M. Frank, Y. Hiçyılmaz, S. Mondal, O. Özdal and C.S. Ün, *Electron and muon magnetic moments and implications for dark matter and model characterisation in non-universal* $\mathrm{U}(1)'$ *supersymmetric models*, *JHEP* **10** (2021) 063 [arXiv:2107.04116] [INSPIRE].

[138] S. Li, Y. Xiao and J.M. Yang, *Can electron and muon* $g-2$ *anomalies be jointly explained in SUSY?*, arXiv:2107.04962 [INSPIRE].

[139] L. Delle Rose, S. Khalil and S. Moretti, *Explaining electron and muon* $g-2$ *anomalies in an Aligned 2-Higgs Doublet Model with right-handed neutrinos*, *Phys. Lett. B* **816** (2021) 136216 [arXiv:2012.06911] [INSPIRE].

[140] F.J. Botella, F. Cornet-Gomez and M. Nebot, *Electron and muon* $g-2$ *anomalies in general flavour conserving two Higgs doublets models*, *Phys. Rev. D* **102** (2020) 035023 [arXiv:2006.01934] [INSPIRE].

[141] S. Jana, V.P.K. and S. Saad, *Resolving electron and muon* $g-2$ *within the 2HDM*, *Phys. Rev. D* **101** (2020) 115037 [arXiv:2003.03386] [INSPIRE].

JHEP03(2022)183

[142] S. Fajfer, J.F. Kamenik and M. Tammaro, *Interplay of New Physics effects in $(g-2)_\ell$ and $h \to \ell^+\ell^-$ — lessons from SMEFT*, *JHEP* **06** (2021) 099 [arXiv:2103.10859] [INSPIRE].

[143] ACME collaboration, *Improved limit on the electric dipole moment of the electron*, *Nature* **562** (2018) 355 [INSPIRE].

[144] MUON $(g-2)$ collaboration, *An Improved Limit on the Muon Electric Dipole Moment*, *Phys. Rev. D* **80** (2009) 052008 [arXiv:0811.1207] [INSPIRE].

[145] M. Abe et al., *A New Approach for Measuring the Muon Anomalous Magnetic Moment and Electric Dipole Moment*, *PTEP* **2019** (2019) 053C02 [arXiv:1901.03047] [INSPIRE].

[146] J-PARC E34 collaboration, *J-PARC Muon $g-2$/EDM experiment*, *JPS Conf. Proc.* **33** (2021) 011110 [INSPIRE].

[147] A. Adelmann et al., *Search for a muon EDM using the frozen-spin technique*, arXiv:2102.08838 [INSPIRE].

[148] L. Wolfenstein, *Neutrino Oscillations in Matter*, *Phys. Rev. D* **17** (1978) 2369 [INSPIRE].

[149] L. Wolfenstein, *Neutrino Oscillations and Stellar Collapse*, *Phys. Rev. D* **20** (1979) 2634 [INSPIRE].

[150] P.S. Bhupal Dev et al., *Neutrino Non-Standard Interactions: A Status Report*, *SciPost Phys. Proc.* **2** (2019) 001 [INSPIRE].

[151] T. Behnke et al. eds., *The International Linear Collider Technical Design Report — Volume 1: Executive Summary*, arXiv:1306.6327 [INSPIRE].

[152] H. Baer et al. eds., *The International Linear Collider Technical Design Report — Volume 2: Physics*, arXiv:1306.6352 [INSPIRE].

[153] C. Adolphsen et al. eds., *The International Linear Collider Technical Design Report — Volume 3.I: Accelerator & in the Technical Design Phase*, arXiv:1306.6353 [INSPIRE].

[154] C. Adolphsen et al., eds., *The International Linear Collider Technical Design Report — Volume 3.II: Accelerator Baseline Design*, arXiv:1306.6328 [INSPIRE].

[155] H. Abramowicz et al., *The International Linear Collider Technical Design Report — Volume 4: Detectors*, arXiv:1306.6329 [INSPIRE].

[156] J.P. Delahaye et al., *Muon Colliders*, arXiv:1901.06150 [INSPIRE].

[157] V. Shiltsev and F. Zimmermann, *Modern and Future Colliders*, *Rev. Mod. Phys.* **93** (2021) 015006 [arXiv:2003.09084] [INSPIRE].

[158] L. Wolfenstein, *A Theoretical Pattern for Neutrino Oscillations*, *Nucl. Phys. B* **175** (1980) 93 [INSPIRE].

[159] T.D. Lee, *A Theory of Spontaneous T Violation*, *Phys. Rev. D* **8** (1973) 1226 [INSPIRE].

[160] G.C. Branco, P.M. Ferreira, L. Lavoura, M.N. Rebelo, M. Sher and J.P. Silva, *Theory and phenomenology of two-Higgs-doublet models*, *Phys. Rept.* **516** (2012) 1 [arXiv:1106.0034] [INSPIRE].

[161] S. Davidson and H.E. Haber, *Basis-independent methods for the two-Higgs-doublet model*, *Phys. Rev. D* **72** (2005) 035004 [*Erratum ibid.* **72** (2005) 099902] [hep-ph/0504050] [INSPIRE].

[162] J.F. Gunion and H.E. Haber, *The CP conserving two Higgs doublet model: The Approach to the decoupling limit*, *Phys. Rev. D* **67** (2003) 075019 [hep-ph/0207010] [INSPIRE].

JHEP03(2022)183

[163] M. Carena, I. Low, N.R. Shah and C.E.M. Wagner, *Impersonating the Standard Model Higgs Boson: Alignment without Decoupling*, *JHEP* **04** (2014) 015 [arXiv:1310.2248] [INSPIRE].

[164] P.S. Bhupal Dev and A. Pilaftsis, *Maximally Symmetric Two Higgs Doublet Model with Natural Standard Model Alignment*, *JHEP* **12** (2014) 024 [*Erratum ibid.* **11** (2015) 147] [arXiv:1408.3405] [INSPIRE].

[165] D. Das and I. Saha, *Search for a stable alignment limit in two-Higgs-doublet models*, *Phys. Rev. D* **91** (2015) 095024 [arXiv:1503.02135] [INSPIRE].

[166] J. Bernon, J.F. Gunion, H.E. Haber, Y. Jiang and S. Kraml, *Scrutinizing the alignment limit in two-Higgs-doublet models: $m_h = 125$ GeV*, *Phys. Rev. D* **92** (2015) 075004 [arXiv:1507.00933] [INSPIRE].

[167] D. Chowdhury and O. Eberhardt, *Update of Global Two-Higgs-Doublet Model Fits*, *JHEP* **05** (2018) 161 [arXiv:1711.02095] [INSPIRE].

[168] K.S. Babu and C.N. Leung, *Classification of effective neutrino mass operators*, *Nucl. Phys. B* **619** (2001) 667 [hep-ph/0106054] [INSPIRE].

[169] A. de Gouvêa and J. Jenkins, *A Survey of Lepton Number Violation Via Effective Operators*, *Phys. Rev. D* **77** (2008) 013008 [arXiv:0708.1344] [INSPIRE].

[170] R. Cepedello, M. Hirsch and J.C. Helo, *Lepton number violating phenomenology of $d = 7$ neutrino mass models*, *JHEP* **01** (2018) 009 [arXiv:1709.03397] [INSPIRE].

[171] J. Gargalionis and R.R. Volkas, *Exploding operators for Majorana neutrino masses and beyond*, *JHEP* **01** (2021) 074 [arXiv:2009.13537] [INSPIRE].

[172] J. Herrero-García, T. Ohlsson, S. Riad and J. Wirén, *Full parameter scan of the Zee model: exploring Higgs lepton flavor violation*, *JHEP* **04** (2017) 130 [arXiv:1701.05345] [INSPIRE].

[173] J. Herrero-Garcia, M. Nebot, N. Rius and A. Santamaria, *The Zee-Babu model revisited in the light of new data*, *Nucl. Phys. B* **885** (2014) 542 [arXiv:1402.4491] [INSPIRE].

[174] A. Ghosal, Y. Koide and H. Fusaoka, *Lepton flavor violating Z decays in the Zee model*, *Phys. Rev. D* **64** (2001) 053012 [hep-ph/0104104] [INSPIRE].

[175] Y. Koide, *Can the Zee model explain the observed neutrino data?*, *Phys. Rev. D* **64** (2001) 077301 [hep-ph/0104226] [INSPIRE].

[176] X.-G. He, *Is the Zee model neutrino mass matrix ruled out?*, *Eur. Phys. J. C* **34** (2004) 371 [hep-ph/0307172] [INSPIRE].

[177] K.S. Babu and J. Julio, *Predictive Model of Radiative Neutrino Masses*, *Phys. Rev. D* **89** (2014) 053004 [arXiv:1310.0303] [INSPIRE].

[178] J.P. Leveille, *The Second Order Weak Correction to $(g-2)$ of the Muon in Arbitrary Gauge Models*, *Nucl. Phys. B* **137** (1978) 63 [INSPIRE].

[179] S.M. Barr and A. Zee, *Electric Dipole Moment of the Electron and of the Neutron*, *Phys. Rev. Lett.* **65** (1990) 21 [*Erratum ibid.* **65** (1990) 2920] [INSPIRE].

[180] J.D. Bjorken and S. Weinberg, *A Mechanism for Nonconservation of Muon Number*, *Phys. Rev. Lett.* **38** (1977) 622 [INSPIRE].

[181] V. Ilisie, *New Barr-Zee contributions to $(g-2)_\mu$ in two-Higgs-doublet models*, *JHEP* **04** (2015) 077 [arXiv:1502.04199] [INSPIRE].

[182] M. Frank and I. Saha, *Muon anomalous magnetic moment in two-Higgs-doublet models with vectorlike leptons*, *Phys. Rev. D* **102** (2020) 115034 [arXiv:2008.11909] [INSPIRE].

JHEP03(2022)183

[183] A. Cherchiglia, P. Kneschke, D. Stöckinger and H. Stöckinger-Kim, *The muon magnetic moment in the 2HDM: complete two-loop result*, *JHEP* **01** (2017) 007 [*Erratum ibid.* **10** (2021) 242] [arXiv:1607.06292] [INSPIRE].

[184] A. Cherchiglia, D. Stöckinger and H. Stöckinger-Kim, *Muon $g-2$ in the 2HDM: maximum results and detailed phenomenology*, *Phys. Rev. D* **98** (2018) 035001 [arXiv:1711.11567] [INSPIRE].

[185] D. Chang, W.-F. Chang, C.-H. Chou and W.-Y. Keung, *Large two loop contributions to $g-2$ from a generic pseudoscalar boson*, *Phys. Rev. D* **63** (2001) 091301 [hep-ph/0009292] [INSPIRE].

[186] G. Ecker, W. Grimus and H. Neufeld, *The Neutron Electric Dipole Moment in Left-right Symmetric Gauge Models*, *Nucl. Phys. B* **229** (1983) 421 [INSPIRE].

[187] BaBar collaboration, *Search for a muonic dark force at BABAR*, *Phys. Rev. D* **94** (2016) 011102 [arXiv:1606.03501] [INSPIRE].

[188] CMS collaboration, *Search for an $L_\mu - L_\tau$ gauge boson using $Z \to 4\mu$ events in proton-proton collisions at $\sqrt{s} = 13$ TeV*, *Phys. Lett. B* **792** (2019) 345 [arXiv:1808.03684] [INSPIRE].

[189] L. Lavoura, *General formulae for $f_1 \to f_2\gamma$*, *Eur. Phys. J. C* **29** (2003) 191 [hep-ph/0302221] [INSPIRE].

[190] MEG collaboration, *Search for the lepton flavour violating decay $\mu^+ \to e^+\gamma$ with the full dataset of the MEG experiment*, *Eur. Phys. J. C* **76** (2016) 434 [arXiv:1605.05081] [INSPIRE].

[191] BaBar collaboration, *Searches for Lepton Flavor Violation in the Decays $\tau^\pm \to e^\pm\gamma$ and $\tau^\pm \to \mu^\pm\gamma$*, *Phys. Rev. Lett.* **104** (2010) 021802 [arXiv:0908.2381] [INSPIRE].

[192] HFLAV collaboration, *Averages of b-hadron, c-hadron, and τ-lepton properties as of summer 2016*, *Eur. Phys. J. C* **77** (2017) 895 [arXiv:1612.07233] [INSPIRE].

[193] SINDRUM collaboration, *Search for the Decay $\mu^+ \to e^+e^+e^-$*, *Nucl. Phys. B* **299** (1988) 1 [INSPIRE].

[194] K. Hayasaka et al., *Search for Lepton Flavor Violating τ Decays into Three Leptons with 719 Million Produced $\tau^+\tau^-$ Pairs*, *Phys. Lett. B* **687** (2010) 139 [arXiv:1001.3221] [INSPIRE].

[195] BaBar collaboration, *Limits on tau Lepton-Flavor Violating Decays in three charged leptons*, *Phys. Rev. D* **81** (2010) 111101 [arXiv:1002.4550] [INSPIRE].

[196] ATLAS collaboration, *Probing lepton flavour violation via neutrinoless $\tau \longrightarrow 3\mu$ decays with the ATLAS detector*, *Eur. Phys. J. C* **76** (2016) 232 [arXiv:1601.03567] [INSPIRE].

[197] LHCb collaboration, *Search for the lepton flavour violating decay $\tau^- \to \mu^-\mu^+\mu^-$*, *JHEP* **02** (2015) 121 [arXiv:1409.8548] [INSPIRE].

[198] M.E. Peskin and T. Takeuchi, *A New constraint on a strongly interacting Higgs sector*, *Phys. Rev. Lett.* **65** (1990) 964 [INSPIRE].

[199] M.E. Peskin and T. Takeuchi, *Estimation of oblique electroweak corrections*, *Phys. Rev. D* **46** (1992) 381 [INSPIRE].

[200] G. Funk, D. O'Neil and R.M. Winters, *What the Oblique Parameters S, T, and U and Their Extensions Reveal About the 2HDM: A Numerical Analysis*, *Int. J. Mod. Phys. A* **27** (2012) 1250021 [arXiv:1110.3812] [INSPIRE].

[201] W. Grimus, L. Lavoura, O.M. Ogreid and P. Osland, *The Oblique parameters in multi-Higgs-doublet models*, *Nucl. Phys. B* **801** (2008) 81 [arXiv:0802.4353] [INSPIRE].

JHEP03(2022)183

[202] B. Pontecorvo, *Mesonium and anti-mesonium*, *Sov. Phys. JETP* **6** (1957) 429 [INSPIRE].

[203] L. Willmann et al., *New bounds from searching for muonium to anti-muonium conversion*, *Phys. Rev. Lett.* **82** (1999) 49 [hep-ex/9807011] [INSPIRE].

[204] U.D. Jentschura, G. Soff, V.G. Ivanov and S.G. Karshenboim, *The Bound $\mu^+\mu^-$ system*, *Phys. Rev. A* **56** (1997) 4483 [physics/9706026] [INSPIRE].

[205] U.D. Jentschura, V.G. Ivanov, G. Soff and S.G. Karshenboim, *Next-to-leading and higher order corrections to the decay rate of dimuonium*, *Phys. Lett. B* **424** (1998) 397 [hep-ph/9706401] [INSPIRE].

[206] I.F. Ginzburg, U.D. Jentschura, S.G. Karshenboim, F. Krauss, V.G. Serbo and G. Soff, *Production of bound $\mu^+\mu^-$ systems in relativistic heavy ion collisions*, *Phys. Rev. C* **58** (1998) 3565 [hep-ph/9805375] [INSPIRE].

[207] T.E. Clark and S.T. Love, *Muonium-anti-muonium oscillations and massive Majorana neutrinos*, *Mod. Phys. Lett. A* **19** (2004) 297 [hep-ph/0307264] [INSPIRE].

[208] R. Harnik, J. Kopp and J. Zupan, *Flavor Violating Higgs Decays*, *JHEP* **03** (2013) 026 [arXiv:1209.1397] [INSPIRE].

[209] P.S.B. Dev, R.N. Mohapatra and Y. Zhang, *Lepton Flavor Violation Induced by a Neutral Scalar at Future Lepton Colliders*, *Phys. Rev. Lett.* **120** (2018) 221804 [arXiv:1711.08430] [INSPIRE].

[210] J. Tang and S. Yat-sen *Search for Muonium to Antimuonium Conversion*, Snowmass2021, Letter of Interest, https://www.snowmass21.org/docs/files/summaries/RF/SNOWMASS21-RF5_RF0_Jian_Tang-126.pdf (2020).

[211] G. Cvetič, C.O. Dib, C.S. Kim and J.D. Kim, *Muonium-antimuonium conversion in models with heavy neutrinos*, *Phys. Rev. D* **71** (2005) 113013 [hep-ph/0504126] [INSPIRE].

[212] C. Han, D. Huang, J. Tang and Y. Zhang, *Probing the doubly charged Higgs boson with a muonium to antimuonium conversion experiment*, *Phys. Rev. D* **103** (2021) 055023 [arXiv:2102.00758] [INSPIRE].

[213] R. Conlin and A.A. Petrov, *Muonium-antimuonium oscillations in effective field theory*, *Phys. Rev. D* **102** (2020) 095001 [arXiv:2005.10276] [INSPIRE].

[214] T. Fukuyama, Y. Mimura and Y. Uesaka, *Models of the muonium to antimuonium transition*, *Phys. Rev. D* **105** (2022) 015026 [arXiv:2108.10736] [INSPIRE].

[215] A. Anastasi et al., *Limit on the production of a low-mass vector boson in $e^+e^- \to U\gamma$, $U \to e^+e^-$ with the KLOE experiment*, *Phys. Lett. B* **750** (2015) 633 [arXiv:1509.00740] [INSPIRE].

[216] D.S.M. Alves and N. Weiner, *A viable QCD axion in the MeV mass range*, *JHEP* **07** (2018) 092 [arXiv:1710.03764] [INSPIRE].

[217] BaBar collaboration, *Search for a Dark Photon in e^+e^- Collisions at BaBar*, *Phys. Rev. Lett.* **113** (2014) 201801 [arXiv:1406.2980] [INSPIRE].

[218] S. Knapen, T. Lin and K.M. Zurek, *Light Dark Matter: Models and Constraints*, *Phys. Rev. D* **96** (2017) 115021 [arXiv:1709.07882] [INSPIRE].

[219] B. Batell, N. Lange, D. McKeen, M. Pospelov and A. Ritz, *Muon anomalous magnetic moment through the leptonic Higgs portal*, *Phys. Rev. D* **95** (2017) 075003 [arXiv:1606.04943] [INSPIRE].

JHEP03(2022)183

[220] B. Batell, A. Freitas, A. Ismail and D. Mckeen, *Flavor-specific scalar mediators*, *Phys. Rev. D* **98** (2018) 055026 [arXiv:1712.10022] [INSPIRE].

[221] LEP, ALEPH, DELPHI, L3 and OPAL collaborations, LEP Electroweak Working Group, SLD Electroweak Group, SLD Heavy Flavor Group, *A Combination of preliminary electroweak measurements and constraints on the standard model*, hep-ex/0312023 [INSPIRE].

[222] N.D. Christensen and C. Duhr, *FeynRules — Feynman rules made easy*, *Comput. Phys. Commun.* **180** (2009) 1614 [arXiv:0806.4194] [INSPIRE].

[223] J. Alwall et al., *The automated computation of tree-level and next-to-leading order differential cross sections, and their matching to parton shower simulations*, *JHEP* **07** (2014) 079 [arXiv:1405.0301] [INSPIRE].

[224] OPAL collaboration, *Tests of the standard model and constraints on new physics from measurements of fermion pair production at 189-GeV to 209-GeV at LEP*, *Eur. Phys. J. C* **33** (2004) 173 [hep-ex/0309053] [INSPIRE].

[225] ALEPH, DELPHI, L3, OPAL and LEP collaborations, *Search for Charged Higgs bosons: Combined Results Using LEP Data*, *Eur. Phys. J. C* **73** (2013) 2463 [arXiv:1301.6065] [INSPIRE].

[226] T. Sjöstrand, S. Mrenna and P.Z. Skands, *PYTHIA 6.4 Physics and Manual*, *JHEP* **05** (2006) 026 [hep-ph/0603175] [INSPIRE].

[227] T. Sjöstrand et al., *An introduction to PYTHIA 8.2*, *Comput. Phys. Commun.* **191** (2015) 159 [arXiv:1410.3012] [INSPIRE].

[228] DELPHES 3 collaboration, *DELPHES 3, A modular framework for fast simulation of a generic collider experiment*, *JHEP* **02** (2014) 057 [arXiv:1307.6346] [INSPIRE].

[229] https://github.com/iLCSoft/ILCDelphes/blob/master/Readme.md.

[230] https://github.com/delphes/delphes/blob/master/cards/delphes_card_MuonColliderDet.tcl.

[231] BELLE-II collaboration, *Belle II Technical Design Report*, arXiv:1011.0352 [INSPIRE].

[232] BELLE-II collaboration, *The Belle II Physics Book*, *PTEP* **2019** (2019) 123C01 [*Erratum ibid.* **2020** (2020) 029201] [arXiv:1808.10567] [INSPIRE].

[233] TEXONO collaboration, *Constraints on Non-Standard Neutrino Interactions and Unparticle Physics with Neutrino-Electron Scattering at the Kuo-Sheng Nuclear Power Reactor*, *Phys. Rev. D* **82** (2010) 033004 [arXiv:1006.1947] [INSPIRE].

[234] I. Esteban, M.C. Gonzalez-Garcia, M. Maltoni, T. Schwetz and A. Zhou, *The fate of hints: updated global analysis of three-flavor neutrino oscillations*, *JHEP* **09** (2020) 178 [arXiv:2007.14792] [INSPIRE].

[235] M. Lindner, M. Platscher and F.S. Queiroz, *A Call for New Physics: The Muon Anomalous Magnetic Moment and Lepton Flavor Violation*, *Phys. Rept.* **731** (2018) 1 [arXiv:1610.06587] [INSPIRE].

JHEP03(2022)183